UNSIVERSITY OF THESSALY

SCHOOL OF ENGINEERING

DEPARTMENT OF MECHANICAL ENGINEERING

Diploma thesis

Fuel Cells: Study of the Cathodic Oxygen Reduction Reaction

by

Molochas I. Konstantinos

Fekas I. Panagiotis

Supervisor

Prof. Tsiakaras Panagiotis

Submitted in fulfillment of the requirements for the Diploma in the Department of Mechanical Engineering of the University of Thessaly

Volos, 2019

ΠΑΝΕΠΙΣΤΗΜΙΟ ΘΕΣΣΑΛΙΑΣ

ΠΟΛΥΤΕΧΝΙΚΗ ΣΧΟΛΗ

ΤΜΗΜΑ ΜΗΧΑΝΟΛΟΓΩΝ ΜΗΧΑΝΙΚΩΝ

Διπλωματική εργασία

Κυψέλες Καυσίμου: Μελέτη της καθοδικής Αντίδρασης της Αναγωγής Οξυγόνου

υπό

Μολόχας Ι. Κωνσταντίνος

Φέκας Ι. Παναγιώτης

Επιβλέπων

Καθηγητής Τσιακάρας Παναγιώτης

Υπεβλήθη για την εκπλήρωση μέρους των απαιτήσεων για την απόκτηση του Διπλώματος Μηχανολόγου Μηχανικού

Βόλος, 2019

Εγκρίθηκε από τα Μέλη της Τριμελούς Εξεταστικής Επιτροπής:

1st Examiner: Dr Tsiakaras Panagiotis (Supervisor)

Professor of Department of Mechanical Engineering,

School of Engineering

University of Thessaly

2nd Examiner: Dr Charalampous Georgios

Assistant Professor of Mechanical Engineering,

School of Engineering

University of Thessaly

3rd Examiner: Dr Angeliki Brouzgou

Senior Researcher and Teaching Staff of Department of Mechanical Engineering,

School of Engineering

University of Thessaly

ACKNOWLEDGEMENTS

Our professor, Dr. Tsiakaras Panagiotis, is the first person we would like to express our gratitude, for his exemplary work as a supervisor and as a mentor. His knowledge, interest, experience, consultation and endless support and encouragement towards us, were some of the tools that helped us through this part of our post-graduate experience. Also, he granting us access at the Laboratory of Alternative Energy Conversion Systems at the Department of Mechanical Engineering in University of Thessaly was a great help for accomplishing our experimental work as well as getting to know the procedures taking place in a real scientific lab.

The lab personnel also deserve a great part of our acknowledgment, Dr Antonios Seretis, Dr Angeliki Brouzgou and Dr Sotiria Kontou, which did not only do a splendid work guiding, assisting and supporting us, but they considered us as a part of the lab and colleagues, making this procedure worth-while and educative for our future steps.

We would like to thankfully express our gratitude to our parents (Panagiotis Fekas to his father Ioannis and his mother Maria and Konstantinos Molochas to his father Ioannis and his mother Anargyri) for the love, the moral and financial support provided, not only during elaborating the present thesis, but also throughout our studies at the Department of Mechanical Engineering in University of Thessaly.

Molochas Konstantinos

Fekas Panagiotis

ABSTRACT

Energy crisis and starvation of commonly used fuels (petroleum, natural gas etch) led to redefining they ways we are storing and utilizing that energy, in need of innovative, adjustable, cheap and environmentally friendly devices. Fuel cells were among the newly proposed devices, mainly for their ability to use hydrogen as a fuel, which is abundant in earth, and secondly because the only by-product, from the chemical reaction taking place, is water. Fuel cells are being investigated by the scientific community for their use in storing energy, as well as their applicability in auto-motive vehicles.

In the first section of this work, general information is provided about the most useful electrochemical devices, among them fuel cells are further analyzed. Next a thorough review on the electrochemistry and thermodynamics, taking place inside a fuel cell, is followed by the explaining of the primary problem of a fuel cell, which is the slow kinetics on its cathode (Oxygen Reduction Reaction).

In the experimental part of this thesis, a series of noble metal (PGM = platinum group metals) catalysts is presented, for the purpose of examining the reaction of the oxygen reduction. Those electrocatalysts consist of pure noble metals (Pt, Pd, Ir) and their alloys (Pt_xPd_y, Pt_xIr_y) supported on carbon Vulcan XC72. A series of electrochemical tests (cyclic voltammetry, linear sweep voltammetry, electrochemical impedance spectroscopy) are conducted in order to determine the properties of the electrocatalysts. By comparing their electrochemical properties, we are able to determine which are suitable for the ORR.

ΠΕΡΙΛΗΨΗ

Η ενεργειακή κρίση και η εξάντληση τον κοινών καυσίμων(πετρέλαιο, φυσικό αέριο κλπ) οδήγησαν στην επαναπροσδιορισμό των τρόπων με τον οποίο αποθηκεύουμε και χρησιμοποιούμε την ενέργεια, με την ανακάλυψη καινοτόμων, προσαρμοστικών, φθηνών και φιλικών προς το περιβάλλον συσκευών. Οι κυψέλες καυσίμων προτάθηκαν κυρίως για την ικανότητα τους να χρησιμοποιούν υδρογόνο σαν καύσιμο, το οποίο είναι άφθονο στον πλανήτη μας, και επίσης διότι το μόνο παραγόμενο κατάλοιπο, από την χημική αντίδραση, είναι το νερό. Οι κυψελίδες καυσίμων ερευνούνται από την επιστημονική κοινότητα για την καταλληλότητα τους σε εφαρμογές αποθήκευσης ενέργειας, καθώς επίσης και στην βιομηχανία των αυτοκινούμενων οχημάτων.

Στο πρώτο κομμάτι αυτής της εργασίας παρέχονται πληροφορίες για τις πιο χρήσιμες ηλεκτροχημικές συσκευές, εκ των οποίων οι κυψελίδες καυσίμων υπόκεινται σε περαιτέρω ανάλυση. Ακολουθεί μία εκτενής ανάλυση στην ηλεκτροχημεία και την θερμοδυναμική, εντός της κυψελίδας καυσίμου, και το θεωρητικό περατώνεται με την επεξήγηση του κύριου προβλήματος των κυψελίδων καυσίμων, δηλαδή την αργή κινητική τους στο κομμάτι της καθόδου (Αναγωγή του Οξυγόνου).

Στο πειραματικό κομμάτι της εργασίας, καταλύτες από ευγενή μέταλλα εξετάζονται για την επιρροή τους στην αντίδραση της Αναγωγής του Οξυγόνου. Οι καταλύτες αποτελούνται από ανόθευτα ευγενή μέταλλα (Pt, Pd, Ir) και από τα κράματα τους (Pt_xPd_y, Pt_xIr_y) πάνω σε άνθρακα Vulcan XC72. Ηλεκτροχημικά τεστ (κυκλική βολταμμετρία, βολταμμετρία ηλεκτροδίου περιστρεφόμενου δίσκου, φασματοσκοπία ηλεκτροχημικής εμπέδησης) διεξάγονται ώστε να προσδιοριστούν οι ιδιότητες των καταλυτών, οι ηλεκτροχημικές αυτές ιδιότητες μελετώνται και συγκρίνονται με σκοπό την επιλογή των κατάλληλων καταλυτών για την υποβοήθηση της αντίδρασης της Αναγωγής του Οξυγόνου.

CONTENTS

LIST OF FIGURES

LIST OF TABLES

CHAPTER I

INTRODUCTION

1.1 Renewable Power Generation Systems

Energy throughout history has been a vital element in human life, from the use of fire in the ancient years, to the industrial revolution in the mid-nineteenth century until nowadays. Today the sustainability of modern societies is completely dependent on the secure, sufficient and accessible supply of energy [1]. The demand for energy provision has increased rapidly in the last decades worldwide and is expected to continue proportionally in the future.

The worldwide electricity generation in 2016 was approximately 16.000 TWh [2], out of which it was estimated that the 57.8% is originated from fossil-fuel-fired plants and 3.2% from biofuels, waste etc. plants, 18% from nuclear plants, 12.8% from hydroelectric plants and only 8.2% from renewable sources [3].

Coal-based electricity generation plants have the highest CO_2 emissions per kWh of electrical power and also other pollutants at high levels. CO_2 is the main cause of ‘’Global Warming Effect’’. Furthermore, fossil fuels are expected to be fully depleted in the next century [4]. Based on these factors, the transition to renewable sources to produce and store the majority of the necessary energy by mid-twentieth first century should be considered for granted, as they have similar or even better performance, and also not emit greenhouse gases [5].

Renewable energy resources are considered as a good alternative solution for the current fossil fuel systems with their minimal emissions and their unlimited availability [6]. The main green renewable power generation systems are photovoltaics, hydropower systems, wind turbines and hydrogen fuel cells. Although these systems contribute to the reduction of energy consumption and emissions, they also represent drawbacks and limitations. For instance, solar and wind energy systems are dependent on weather conditions, so they display wide variations in their output power, while hydropower rely on water availability and geographic position. The disadvantages of these systems can be overcome by combining them together. For

example, photovoltaics and wind turbines can compose a hybrid renewable energy system using an energy-storage system such as batteries and fuel cells [7].

Unlike other renewable energy systems, fuel cells are not depended on geographic position or weather conditions. In addition, fuel cells are part of the hydrogen energy economy. Hydrogen is considered an attractive alternative fuel, because its only by-product is water when it reacts with air in a fuel cell. Furthermore, they can be applied in most areas of applications, like portable power, stationary plants and transportations with benefits over batteries, internal combustion engines and other current power generation systems [7]. Therefore, fuel cell technology and hydrogen are going to play a crucial role in the effort of reducing greenhouse gases emissions, and the dependence on fossil fuels.

1.2 Electrochemical Cells and Reactions

Electrochemistry is the branch of chemistry concerned with the interaction between electrical and chemical effects [8]. More precisely, it deals with the study of chemical changes caused by the passage of electrical current and the production of electrical power by chemical reactions. Electroanalytical chemistry analyzes the properties of the electrochemical reactions that take place in an electrochemical process. The electrochemical process that an electrochemical device follows, and its structure can be generally presented by the analysis of a typical electrochemical cell.

An electrochemical cell is a system consisting of electrodes that dip into an electrolyte and in which a chemical reaction either uses or generates an electrical current [9]. It consists of two half-cells which are electrically connected, and on each of them an electrochemical reaction occurs. A half-cell consists of a metal strip that dips into a solution of its metal ion. A typical example of an electrochemical cell is the Daniell cell which is constructed in 1836 by the English chemist John Frederick Daniell [9]. An atomic view of Daniell cell is represented in Fig. 1.1.

As depicted, the electrochemical cell is made of a zinc-zinc ion half-cell (zinc electrode) and a copper-copper ion half-cell (copper electrode) that are connected with a salt bridge. At the zinc electrode oxidation occurs, meaning that zinc atoms lose electrons to produce zinc ions. Electrons flow through an external circuit to the copper electrode, producing electrical current. There, the electrons react with the copper ions to deposit copper atoms.

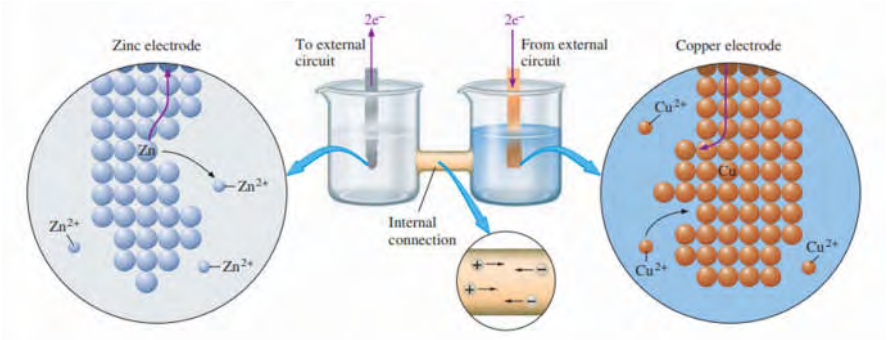

Figure 1.1 An atomic view of Daniell cell [9].

The salt bridge, which connects the two half-cells, is a tube of an electrolyte that allows the flow of ions but insulates the mixing of different solutions. If the positive ions do not flow from the one electrode to the other, the half-cell reactions will stop. Also, the two solutions should not mix because a direct reaction will occur without the generation of electrical current. The half-reactions at each electrode and the overall reaction of the cell are given as below [9].

Anode (oxidation half-reaction): $Zn(s) \rightarrow Zn^{2+}(aq) + 2e^{-}$ (1.1)

Cathode (reduction half-reaction): $Cu^{2+}(aq) + 2e^{-} \rightarrow Cu(s)$ (1.2)

Overall: $Zn(s) + Cu^{2+}(aq) \rightarrow Zn^{2+}(aq) + Cu(s)$ (1.3)

After the presentation of the main parts and the operation principles of the electrochemical cell, a distinction between voltaic cell and electrolytic cell should be made. A voltaic or galvanic cell is an electrochemical cell in which a spontaneous reaction produces an electrical current [9] Note that Daniell cell is a voltaic cell, because the anode is the zinc electrode. Zinc tends to lose electrons more easily than copper, so the oxidation occurs spontaneously. Therefore, a voltaic cell produces potential to run an external load. The anode has a negative sign, because electrons flow from it, and respectively the cathode has a positive sign. On the contrary, an electrolytic cell is an electrochemical cell in which an electrical current drives a nonspontaneous reaction [9]. In this case an external current is consumed. Electrolytic cells are used to process material electrochemically. A typical example is the electrolysis of water. Unlike voltaic cell, here the anode has a positive sign and the cathode a negative sign.

CHAPTER II

ELECTROCHEMICAL DEVICES

2.1 Supercapacitors

A Supercapacitor (SC), also known as ultracapacitor, is basically a device used for storage of electric energy. Specifically, it is a combination of 2 other devices used for storage, batteries and normal capacitors. Their differences and similarities sum up to four categories: 1) Specific Energy (Wh/kg), 2) Specific Power (W/kg), 3) Discharge-charge time, 4) Cycle life.

SC have low Specific Energy compared to batteries, about 3-30 times lower [10], meaning they can't store as much charge as batteries can, this is alleviated by the fact their Specific Power is larger than this of batteries. Compared to capacitors, SC have lower power output but their Specific Energy is several magnitudes larger than this of capacitors [11]. All the previous remarks are illustrated in Fig. 2.1. Discharge-charge time in SC is a matter of seconds, a capacitor needs fractions of seconds, but a battery requires several hours to fully discharge-charge.

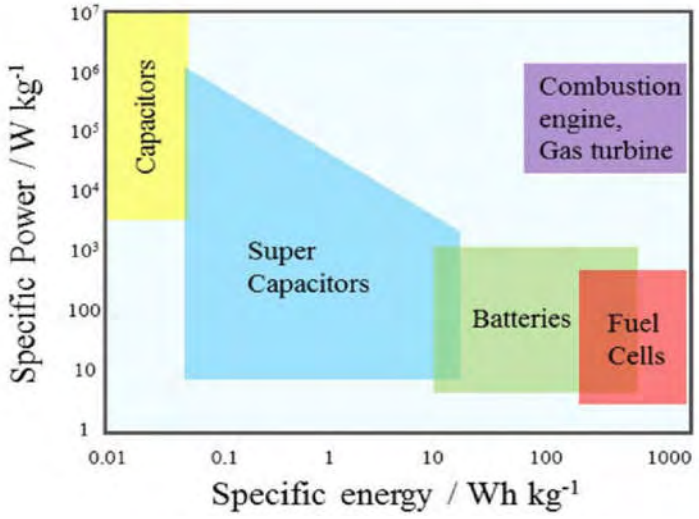

Figure 2.1 Ragone plot comparing electrochemical systems and internal combustion engines [12].

Cycle-life is another area where SC are superior to batteries, because they can last up to hundreds of thousands, even millions, cycles which is large compared to the

thousands cycles of life batteries possess [13]. Finally, SC can operate in wider temperature ranges and at the same time be safer than batteries, because they don't involve chemical reactions on metals. Their main disadvantage, except from low Specific Energy, is that SC usually operates at low voltages, around 1-3 V. Higher voltages can be reached by connecting SC is a series but that leads to a problem with space and weight [14].

Supercapacitors store energy via two mechanisms (Fig.2.2):

i) Electrochemical Double Layer Capacitance, electrostatic storage of electric energy achieved by separation of oppositely charged species in a Helmholtz double layer, surrounding the surface of electrode.

ii) Pseudo-capacitance, electrochemical storage of electric energy achieved by Faradaic RedOx reactions across the electrolyte-electrode interface.

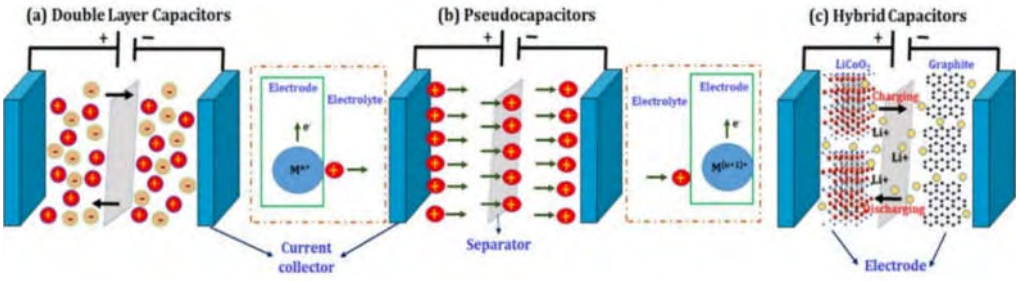

Figure 2.2 Different types of Supercapacitors depending on the energy storage mechanism [15].

A SC consists of two electrodes, coated with highly porous materials, an ion-permeable membrane and an electrolyte ionically connecting electrodes.

The electrode materials usually are carbon-based materials, metal oxides or conducting polymers. These materials need to possess 1) high specific surface area, 2) controlled porosity, 3) high electronic conductivity, 4) desirable electroactive sites, 5) high thermal and chemical stability, last and not least 6) low cost [16].

Membranes need to be ion-permeable, have high electrical resistance, high ionic conductance and low thickness. Their materials are usually affected by the selection of the electrolyte, meaning polymer or paper separators are used with organic electrolytes and ceramic or glass fiber membranes are paired with aqueous electrolytes.

Electrolyte is also important for the SC; low concentrations can starve the cell and reduce the performance. Conductivity and the temperature coefficient are two

important factors that have to be considered when selecting an electrolyte. The majority of electrolytes are aqueous and organic, ionic liquids are used too [13].

Their properties can be matched with these of convectional capacitors, capacitance C, equation (2.1), depends on effective thickness of the double layer d, A is the specific surface area of electrodes, ε_o is the dielectric constant of the vacuum and ε_r the dielectric constant of the electrolyte.

$$C = \frac{\varepsilon_o \varepsilon_r}{d} A \tag{2.1}$$

$$E = \frac{CV^2}{2} \tag{2.2}$$

$$P_{max} = \frac{V^2}{4R} \tag{2.3}$$

Equations (2.2) and (2.3) express, respectively, the energy density of a SC (V refers to cell voltage) and the maximum power density of the SC (R refers to internal resistance of the device).

Some of SC applications involve Dynamic Breaking System, photographic flashes, MP3 players, static memories (SRAM), wind turbines (smoothing out the intermittent power supplied by wind), train and buses acceleration, burst power for lifting operations, backup power system [14]. Supercapacitors are not meant be a replacement for batteries, but instead supercapacitors are ideal when quick charge-discharge is needed. Usually they are combined with batteries.

2.2 Electrochemical Sensors

Electrochemical sensors are devices that detect oxygen, and other gases of interest, by producing an electrical signal proportional to the gas concentration. What makes electrochemical sensors preferable, compared to thermal and optical sensors, is their good detectability. Typically, an electrochemical sensor, Fig. 2.3, is consisted of i) gas permeable membrane (diffusion barrier) which is used to control the amount of gas molecules and determine the size of the particles reaching electrode (capillary effect), depending on the gas we want to detect. It also possesses ii) a working-sensing electrode, a counter electrode and a reference electrode with stable potential in order to monitor the change in working electrode's onset potential; electrodes usually are made of noble metals. Finally, iii) an electrolyte allows the transfer of ions among electrodes, electrolytes are usually aqueous or liquid, but solid electrolytes are

used when working conditions require a temperature above 500°C. Electrochemical sensors can operate in a wide temperature range of -30°C up to 1600°C [17].

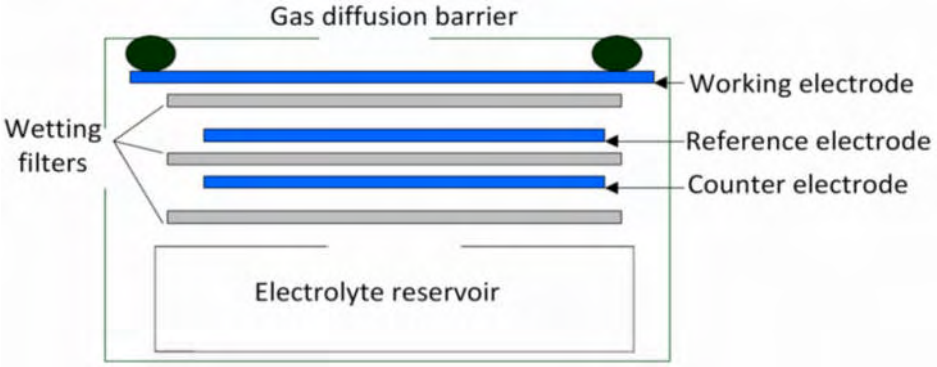

Figure 2.3 Schematic representation of an electrochemical gas sensor [18].

There are 3 major types of electrochemical sensors [19-21]:

A) Potentiometric Sensors

These sensors detect gases by comparing working electrode's surface potential, which is related to the activity of dissolved ions, with a reference electrode. The relation between concentration and potential is affiliated with Nernst equation. A selective ion-conductive membrane is needed, in order to allow the preferable gas to pass. Potentiometric sensors are used in a big excess, because of their simple instrumentation, low cost, continuous monitoring combined with a long lifetime and good mechanical stability. The most used potentiometric device is the pH electrode.

B) Amperometric Sensors

They are further categorized depending on how current is measured, amperometric sensors use a steady potential, while voltametric sensor's current is measured for a scanning range of potentials. Their most important component is the working electrode, where the oxidation-reduction of the electroactive species takes place. That's why most of the research is focused on finding better materials, in a matter of stability, cost and durability for the electrode. Amperometric sensors are the footing of biosensors, resulting from the development of microelectrodes.

C) Conductometric Sensors

These sensors measure the ability of a bulk material, affected by the electrolyte in use, to conduct an electrical current between electrodes. The

absence of a reference electrode makes them simpler and more cost efficient. They are often used as gas detecting sensors.

Electrochemical sensor's main advantages focus on their good selectivity, repeatability, accuracy and of course low cost (materials and power consumption). Still they are some drawbacks that needed to be taken in mind, like their sensitivity in temperature and pressure changes, electrolyte leakage or dryness. These sensors also can be poisoned by an unwanted gas, leading to deterioration of their performance or permanently destroying them. Finally, they have a limited lifetime, independent from what mentioned above, around 1-3 years [20].

2.3 Batteries

Batteries basically are electrochemical cells connected in a series or parallel. An electrochemical cell is consisted of a positive charged electrode called 'anode' and a negative charged electrode called 'cathode', emerged in an electrolyte and frequently separated by an ion permeable membrane. They convert chemical stored energy to electrical, when demanded, through RedOx reactions taking place on electrodes [22]. More analytically, electrical energy is produced by the movement of electrons from anode, where oxidation takes place, to cathode where the electroactive species are being reduced, Fig. 2.4. These electroactive species which exist within the electrolyte and the membrane, mentioned above, are used to prevent electrons transferring instinctively in the electrolyte without passing through the electrodes. The electrodes are usually made of metals or metal oxides, which enhance the properties needed so electron transfer take place. Electrolytes can be liquid (aqueous or non-aqueous) or solid. Batteries can be divided in Primary batteries and Secondary-Rechargeable batteries, based on the times used.

Primary batteries can be used only for a single time because their discharge reaction isn't reversible, that's the result of very stable products. Common types: Carbon Zinc, Alkaline, Lithium Cells, Silver Oxide Cells, Zinc Air Cells.

Secondary batteries can be recharged and discharged several times, when they are fully discharged electric current is applied to force them into their original state. However, they can't charge-discharge infinite times, because of the deterioration of the metals for every charge-discharge cycle, leading to reduction in capacity of the

battery. Common types: Alkaline, Nickel-Cadmium, Nickel-Metal Hydride, Lithium Ion, Lead Acid [23].

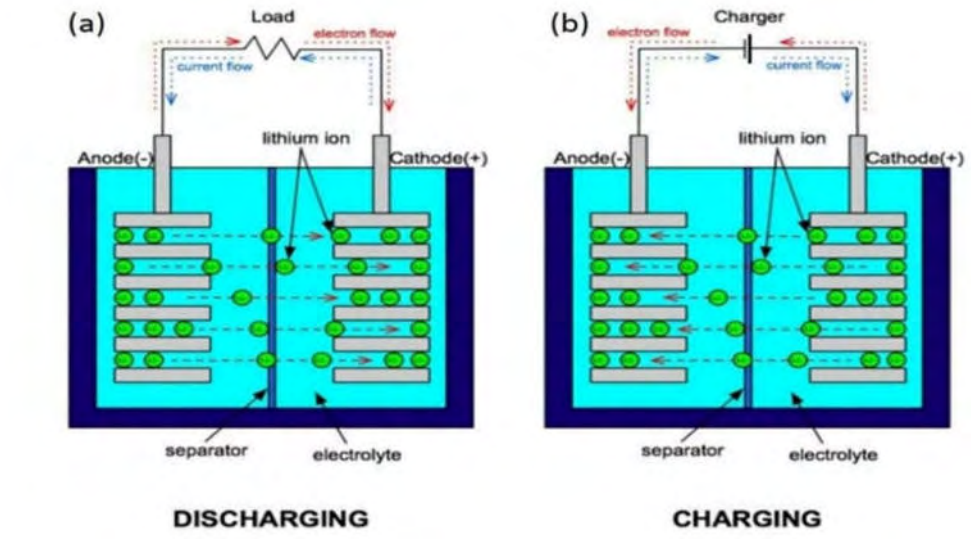

Figure 2.4 Schematic diagram of a battery's electroactive species, during a) Discharging and b) Charging [24].

Most of the research and development part concerning batteries is focused on rechargeable Li-ion batteries, and overall Lithium based batteries, due to their high specific energy and energy density. A Li-ion battery usually operates on 4 V with specific energy between 100 Wh/kg and 150 Wh/kg [25]. These cells typically consist of a grapheme anode, a lithium metal oxide cathode and solution of lithium salt serving as the electrolyte. Li-ion batteries today are commonly used for portable devices, such as laptop, cellphones etch, but still there are many aspects they need to improve so they institutionalize themselves on the electronics market. Cycle life and safety are some of their disadvantages and are mostly dependent on the choice of electrode and electrolyte materials [26]. Batteries generally, in order to cope with market demand and fulfil their role as the energy storage device of the future, they have to improve on several tasks including specific energy, specific power, cost, safety, reliability and material availability.

CHAPTER III

FUEL CELLS

3.1 Historical Overview

In 1800 the British scientists William Nicholson and Sir Antony Carlisle discovered the process of electrolysis, in which water is decomposed into hydrogen and oxygen by the use of electricity. Based on this idea, in 1838 Sir William Grove, a Welsh judge, inventor and physical scientist, invented the ‘’gas battery’’, a fifty-fuel cell stack [27]. More precisely, he found that electrolysis could be performed in reverse with the appropriate catalyst to produce electricity. Although many scientists had achieved to update Grove’s idea in scientific level, for almost a century the fuel cells did not progress practically.

Francis Thomas Bacon, an English engineer, was the first to develop a fuel cell with practical use. In 1958 Bacon presented an alkaline fuel cell to Britain’s National Research Development Corporation. Even though their construction cost was high, Bacon’s cells were proved to be exceptionally reliable. In the early 1960s Thomas Grubb and Leonard Niedrach, chemists of General Electric (GE), invented the Polymer Exchange Membrane fuel cell (PEMFC), which exhibited high efficiency and durability. GE’s fuel cell technology was used for U.S space programs, such as Gemini and Apollo spacecrafts [28].

Until the late 1980s, fuel cell applications were limited for space missions due to their high cost. From the early 1990s until nowadays, there have been attempts to commercialize fuel cells on transportation, portable and stationary power generation, although yet it is not possible due to restrictions on generation and storage of hydrogen, besides the high production cost of the fuel cells [28]. Today, the scientific research focuses on optimizing the efficiency, durability, stability and cost of the fuel cells, although improvements in hydrogen generation and storage are also required. In Fig. 3.1 an extensive historical review of fuel cells is depicted, from 1800 to 2007.

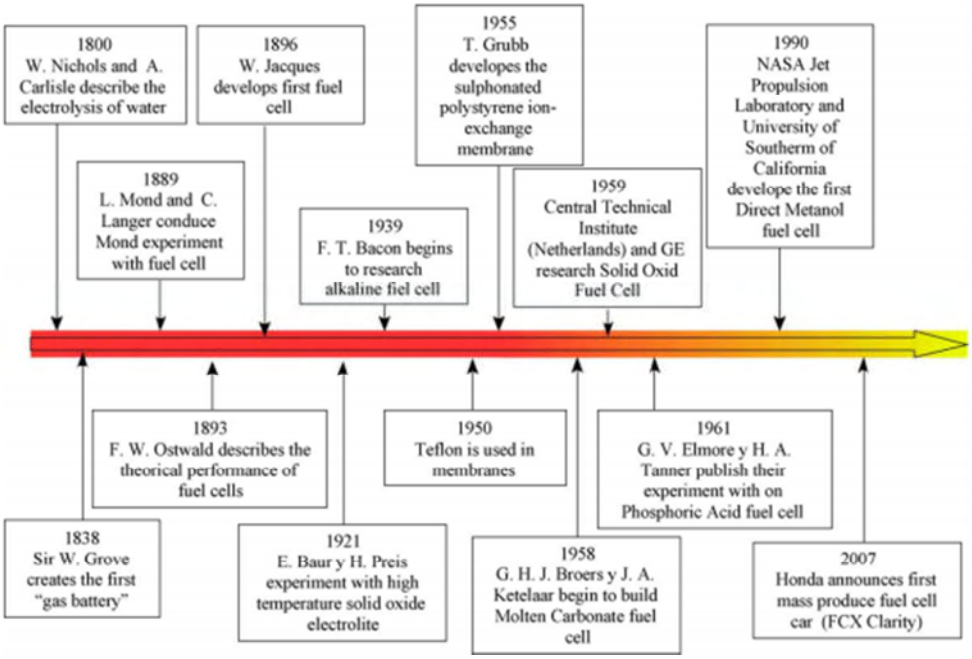

Figure 3.1 Historical review of fuel cells [28].

3.2 Basic Working Principles

A fuel cell is an electrochemical device that continuously and directly converts the chemical energy of the externally supplied fuel and oxidant to electricity [29]. Practically, internal combustion is replaced by more efficient and non-polluting energy source. Like electrochemical reactors, fuel cells consist of two electrodes, the anode and the cathode, where electrochemical reactions take place, and an electrolyte between them. Anode is the negative electrode, where the fuel is delivered and oxidized, and respectively cathode is the positive electrode, where the oxidant, oxygen in most cases, is supplied and reduced [30]. The electrolyte separates the two electrodes and prevents their direct contact; also allows the transportation of the ionic species between the electrodes, while at the same time blocks the electron transfer through it [31].

In Fig. 3.2 a typical hydrogen-oxygen fuel cell is shown. Hydrogen is supplied at the anode, where it is decomposed into positive charged protons and negative charged electrons. The electrolyte between the electrodes permits only the positive ions to flow from the anode to cathode, and concurrently insulates electrons from transferring through it. In order for the system to be stable, the electrons are forced to travel through an external circuit, producing electrical current. At the cathode, protons and electrons are remerged, together with oxygen, to form pure water as the only byproduct [32].

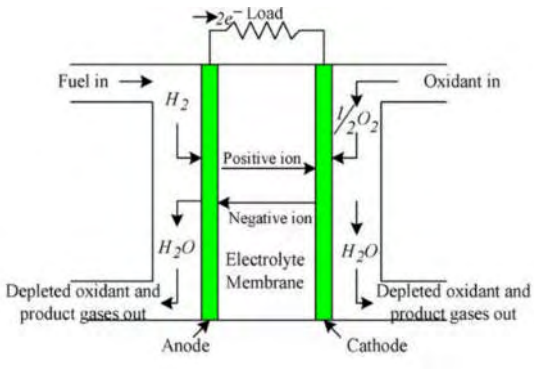

Figure 3.2 Fuel cell operation diagram [32].

The hydrogen oxidation reaction (HOR) and the oxygen reduction reaction (ORR) at the two electrodes, are facilitated by the presence of a catalyst. The half reactions involved at each electrode and its overall reaction are given as below.

Anode reaction: $$H_2 \rightarrow 2H^+ + 2e^-$$ (2.1)

Cathode reaction: $$2H^+ + ½O_2 + 2e^- \rightarrow H_2O$$ (2.2)

Overall reaction: $$H_2 + ½\, O_2 \rightarrow H_2O$$ (2.3)

At this point, a distinction between fuel cells and batteries should be made. Both fuel cells and batteries convert chemical energy directly into electrical energy. However, batteries are energy-storage devices, while fuel cells are energy-producing devices. More specifically, batteries store the reactants inside them and when they use them up, they are discharged. If the battery is primary, it is discharged after the consumption of the active materials, while if it is secondary, it can be recharged by electricity and reused. At fuel cells, the fuel and the oxidant are supplied from external sources, and they can operate continuously as long as they fed with the reactants [7].

3.3 Classification of Fuel Cells

Fuel cells are classified according to the material used for the electrolyte. The type of the electrolyte determines the operating temperature, the fuel used and therefore the application of the fuel cells. The five types of fuel cells are the following [7]:

- Alkaline fuel cells (AFC)
- Molten carbonate fuel cells (MCFC)
- Phosphoric acid fuel cells (PAFC)
- Proton-exchange membrane fuel cells (PEMFC)
- Solid oxide fuel cells (SOFC)

Table 3.1 lists the main properties of each type.

Table 3.1 Types of fuel cells and their main properties [7].

	AFC	MCFC	PAFC	PEMFC	SOFC
Electrolyte	Potassium hydroxide	Immobilized liquid molten carbonate	Immobilized liquid phosphoric acid	Ion exchange membrane	Ceramic
Operating temperature	60-250^{0}C	500-650^{o}C	120-210^{o}C	20-80^{o}C	750-1000^{o}C
Mobile ion	OH^-	CO_3^{2-}	H^+	H^+	O^{2-}
Efficiency	45-60%	45-60%	35-40%	40-60%	50-65%
Possible applications	Submarine, spaceships	Power stations	Power stations	Vehicles, portable	Power stations, portable
Electrical power	10-100 kW	0.3-3 MW	400 kW	250 kW	1-3 MW

3.4 Proton-Exchange Membrane Fuel Cells (PEMFC)

Proton-exchange membrane fuel cells (PEMFC), are considered future power sources for portable applications and transportation, due to their low operation temperature, high power density and their high energy efficiency [29]. Furthermore, PEM fuel cells convert hydrogen and oxygen into electricity via electrochemical process, with water being the only byproduct, so they are characterized by minimal environmental impact.

A single PEM fuel cell consists of one anode and one cathode with the polymer electrolyte in contact with them. In this case the operating voltage of the cell is approximately 0.6 V, which is not enough to power most industrial devices. In order to increase the performance, multiple single cells are stacked together in parallel and/or in series, creating a fuel cell stack. In practical applications stacks are part of fuel cell systems, which also include hydrogen reformer, air supply module, water manager module and thermal manager module [29]. The arrangement of the system varies, depending on the application, the fuel cell type and the fuel used.

3.4.1 Cell Components and Materials

The main components of a PEM fuel cell, which can be distinguished in Fig. 3.3, are the membrane-electrode assembly (MEA) and bipolar plates. MEA is the key part of the cell, which consists of a proton exchange membrane, a gas diffusion layer and a dispersed catalyst layer [33]. Each component should accommodate the required properties and functions; therefore, the design and manufacturing conditions should be carefully considered.

- Proton exchange membrane

The membrane is placed between the two catalyst layers of the electrodes and separates the oxidation and reduction half reactions. It allows protons to pass through, while at the same time it blocks electrons from doing so, forcing them to flow through an external circuit. The main required properties of the membrane are thermal stability, ionic conductivity, chemical and flow reactant permeability and durability [31, 34]. The types of material that can achieve those properties are Perfluorinated, partially fluorinated, non-fluorinates and non-fluorinated composites [33].

- Catalyst layers

The main function of catalyst layers is the stimulation of electrochemical reactions at each electrode. They must be catalytic active for both hydrogen oxidation reaction (HOR) and oxygen reduction reaction (ORR), durable and electrochemically stable. The best catalyst that satisfy those requirements is Pt and its alloys. However, they have also been fabricated non-Pt-based catalysts that achieve efficient reaction rates [31, 35].

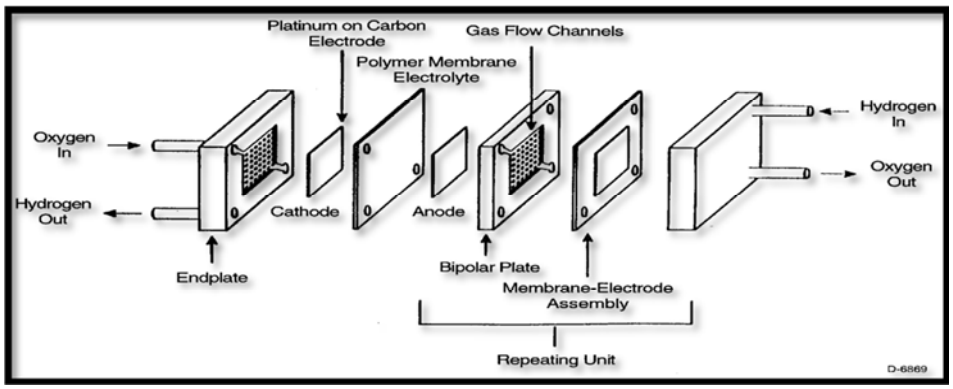

Figure 3.3 PEM fuel cell components [36].

- Gas diffusion layers

The functions of gas diffusion layers are to transport the reactant gases from flow channels to catalyst layers effectively, drain out water from catalyst layers to flow channels, conduct electrons with low resistance and keep the membrane in wet condition at low humidity [37]. The parameters that should be optimized are porosity, thickness, diameter of fiber and polytetrafluoroethylene (PTEE) loading of gas diffusion layers, in order to be efficient. The materials used should be permeable, electronically conductive, compressible and possess balanced hydrophobicity and hydrophilicity [38].

- Bipolar plates

Bipolar plates account for the highest portion of fuel cell weight and almost half the total cost. Their main functions are to distribute reactants uniformly, facilitate heat management, separate the individual cells in the stack, prevent the leakage of coolant and reactants and facilitate water management within the cell. The used materials should have the following properties: corrosion resistance, chemical stability, thermal conductivity, hydrophobicity, compressive strength and electrical conductivity. The required properties are achieved by of non-porous graphite, metals such as aluminum, stainless steel, nickel and titanium, as well as polymer composites (metal or carbon-based) [39].

3.4.2 Performance Degradation and Failure Modes

Inside the fuel cell may occur several faults, such as chemical, electrochemical, mechanical and electrical faults. Those faults lead to degradation at each component, affecting the durability and the performance of the cell. On Table 3.2 the basic failure modes and degradations are summarized.

Table 3.2 Failure modes and degradations of PEM fuel cell components [7, 29].

Component	Failure modes	Causes
Membrane	-Thermal degradation -Chemical/electrochemical degradation -Mechanical degradation	-Thermal stress -Thermal cycles -Impurities contamination -Radical attack -Mechanical stress because of non-uniform press pressure -Inadequate humidification or penetration of the catalyst and seal material -Traces
Catalyst layer	-Loss of activation -Loss of conductivity -Decrease in mass transport rate of reactants -Loss of reformate tolerance -Decrease in water management ability	-Sintering or de-alloying of catalyst -Corrosion of electrocatalyst support -Mechanical stress -Contamination -Change in hydrophobicity of materials due to Nafion or PTFE dissolution
Gas diffusion layer	-Decrease in mass transport -Decrease in water management ability -Conductivity loss	-Degradation of backing material -Mechanical stress change in the hydrophobicity of materials -Corrosion
Bipolar plates	-Fracture/deformation -Mechanical failure -Loss of conductivity	-Mechanical stress -Corrosion -Mechanical stress -Corrosion, oxidation

3.4.3 Operation Principles and Conditions

The PEM fuel cell operation involves multiple phenomena, such as heat transfer, charge and species transport, fluid flows and electrochemical reactions. The working principle is shown in Fig. 3.4 in two-dimensional view and it is composed of the following steps [40]:

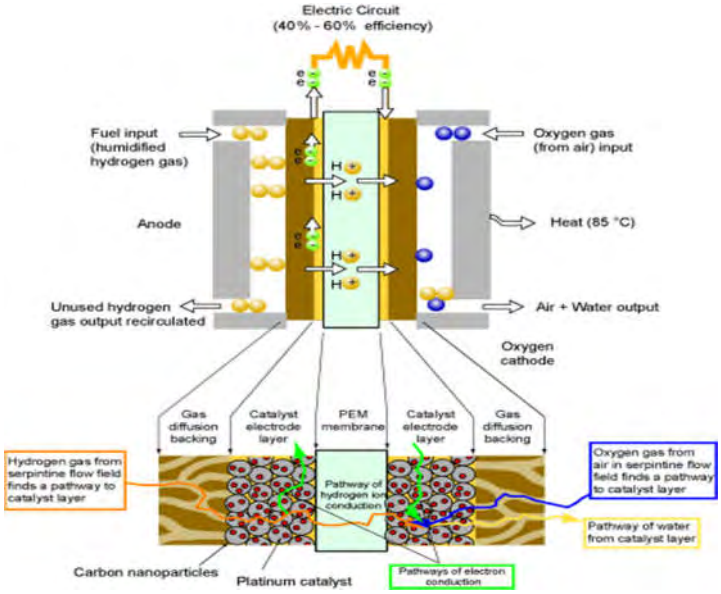

Figure 3.4 Phenomena in a PEM fuel cell [40].

1. Air and hydrogen gas are fed to the cathode and anode gas flow channels respectively.
2. Hydrogen and oxygen flow through the porous gas diffusion layers and diffuse into the respective catalyst layers.
3. At the anode catalyst layer, hydrogen is oxidized, decomposing into electrons and protons.
4. Protons transfer, and water is supplied through the membrane.
5. Electrons are conducted to the anode current collector, and then to the cathode current collector via an external circuit.
6. Oxygen is reduced at the cathode catalyst layer with protons and electrons, forming water.
7. Water is extruded from the cathode catalyst layer, through the cathode gas diffusion layer, and finally out of the cathode gas flow channel.
8. Because of degradations, and mainly due to the sluggish oxygen reduction reaction (ORR) in the cathode catalyst layer, heat is generated. Bipolar plates contribute to the conduction of heat out of the cell.

The fuel cell power output depends on operation conditions, such as gas flow, operating pressure and temperature, generated heat, as well as water management. More specifically, pressure is equivalent to efficiency and conversely equivalent to compressor power, and it is also dependent on water management, so it must be optimized. The same applies to operating temperature, which is equivalent to cell potential, and therefore to performance, but it is also related to the heat management. The reactions that occur to fuel cells are exothermic, therefore, to maintain the temperature at its desired value, a cooling system must transport the generated heat out of the cell. The coolant medium may be water, air or a special industrial coolant. As for water management, it is closely related to the performance and durability of PEM fuel cells. More precisely, water management must maintain the humidity of the reactants to optimum levels, in order for the membrane to be sufficiently hydrated, since the conductivity of the membrane is directly related to its hydration [29, 40].

3.5 Fuel Cell Applications

Fuel cells, due to their high efficiency and zero greenhouse gas emissions, are expected to be the key technology for future applications, replacing the internal combustion engines at hydrogen economy era. Furthermore, proportionally to the type of fuel cell, they cover a wide range of output power and operation temperatures, therefore they can be applied to many areas of applications. Fuel cell applications can be classified into four main groups: stationary power, transportation, portable power and backup power [29].

- Stationary power

For over twenty years, fuel cells have been commercialized for stationary applications. Those fuel cell systems show differences in the type of fuel cell, the fuel used and the cooling and heating of the stacks. The fuel cell system can either be connected to the grid to provide additional electrical power to the plant, or as an independent grid system, for remote or isolated areas. Stationary power systems based on fuel cells today can achieve approximately an efficiency of 40%, using hydrocarbon as a fuel, and taking as starting point the fuel and as end point the generated electricity [40]. Fuel cells also can be connected with photovoltaics, wind turbines, batteries and capacitors, providing primary or secondary power. Co-generation increases the efficiency up to 85% while reducing energy consumption [7].

- Transportation

Fuel cell vehicles are considered as the ‘’next generation’’ technology because they are highly efficient, silent and they lead to low emissions if the hydrogen is produced from fossil fuel, compared to internal combustion engines, or even zero emissions if the hydrogen is produced from renewable sources. Fuel cells have been applied to automobiles, motorcycles, mining trains, aircrafts and ships for the military and to long-haul trucks as auxiliary power units. PEM fuel cells are probable the most suitable for transportation applications due to their low operating temperature, their power density, and their high efficiency [29].

- Portable power

Batteries are expected to be replaced in the near future by PEM fuel cells and direct methanol fuel cells (DMFC) on portable electronic devices, such as laptop computers, cell phones etc. Fuel cells can achieve higher power and energy capacity than batteries, which are characterized by limited capacity and slow recharging [29]. Moreover, fuel cells operate at a constant level for as long as they are fed with fuel, unlike batteries which their performance is degraded when the charge level drops. The most promising type of fuel cell for those applications is DMFC, because it is inexpensive and do not require hydrogen gas as fuel [40, 41].

- Backup power

Backup systems provide power when the primary source is interrupted. The main required properties for a backup power device are availability and reliability. The most common used power providers today are engine generators, valve-regulated lead-acid battery systems, ultra-capacitors, flywheels and most recently fuel cells have joined the group [29]. Normally the preferred fuel used is hydrogen, compared to a reformate hydrocarbon, because the main requirement of a backup power system is to start instantly. Furthermore, a short system lifetime is required, as backup devices are used as intermediate power sources, therefore the operation lifetime for the fuel cell is less than 2000 hours [41]. Based on those factors we can deduce that backup power is going to be the first commercialized application of the fuel cells.

CHAPTER IV

OXYGEN REDUCTION REACTION (ORR)

4.1 Basic Reactions

A Proton Exchange Membrane (PEM) fuel cell comprises 2 electrodes, an electric circuit, an electrolyte and a polymer membrane in order to produce electric energy. The fuel, hydrogen, is provided to the electrode called anode. There a reaction, called Hydrogen Oxidation Reaction (HOR), takes places so hydrogen can be stripped from its electrons.

$$2H_2 \rightarrow 4H^+ + 4e^- \qquad E^o=0.00V \qquad (4.1)$$

On the other side-electrode of PEM fuel cell, called cathode, a different reaction is taking place. With the assistance of the oxygen provided, the electrons inside the circuit interact with oxygen and hydrogen cations, which are transferred from the anode through the membrane to the cathode, so water is produced.

$$O_2 + 4e^- + 4H^+ \rightarrow 2H_2O \qquad E^o=1.229V \qquad (4.2)$$

The above is called Oxygen Reduction Reaction (ORR)

Overall reaction: $H_2 + 1/2O_2 \rightarrow H_2O$ $\Delta E=1.229V$ (4.3)

Electron's oriented motion through the circuit is what causes electric energy to be produced [42].

Comparing HOR and ORR, one can determine than the kinetics involved around ORR are slower than of HOR. The truth is that oxygen reduction reaction is about 5 orders slower than hydrogen oxidation reaction, which leads to the need of finding ways of enhancing the kinetics of ORR without interfering with the cathode or the overall function of the PEM fuel cell. For example, if our electrodes were made out of Pt, then anode could have a catalyst loading of 0.05 mg cm^{-2} or less, while cathode would need approximately 0.4 mg cm^{-2} [43, 44].

Even though the reaction for ORR looks simply, in the reality it is very complicated and involves numerous elementary steps and intermediate species. The

fact that ORR has an activation potential close to the onset potential, and the lack of proper experimental techniques and equipment, make it hard to study it. Fig. 4.1 illustrates the phenomenon of early activation potential, leading to mass transfer-controlled region appearing too soon and obstructing the research of electron mechanism [45, 46].

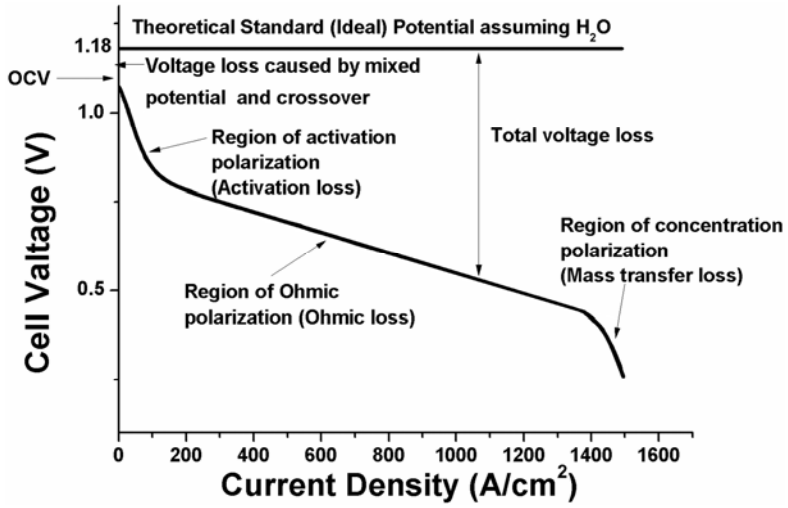

Figure 4.1 Illustration of loses during a linear sweep voltammogram for the ORR, depending on the overpotential [47].

In fact, it is considered that the first electron transfer is the rate determining step for ORR. Other steps have also been reported to slow down ORR such as, desorption of the intermediates or the hydration of oxygen [48]. A scheme, Fig. 4.2, is used in order to simplify the ORR kinetics. From this scheme we can deduce that [48]:

1. Oxygen can be directly reduced to water through a 4-electron reaction mechanism.
2. Oxygen getting reduced to intermediate species, hydrogen peroxide, through a 2-electron reaction.
3. Hydrogen peroxide can follow multiple paths, it can be further reduced to water involving 2 more electrons, or it can be oxidized back to oxygen.
4. It can also be decomposed in water and oxygen, a catalytic (non-electrochemical) reaction.
5. Finally, hydrogen peroxide could go through desorption into the bulk, or adsorption back to the catalyst.

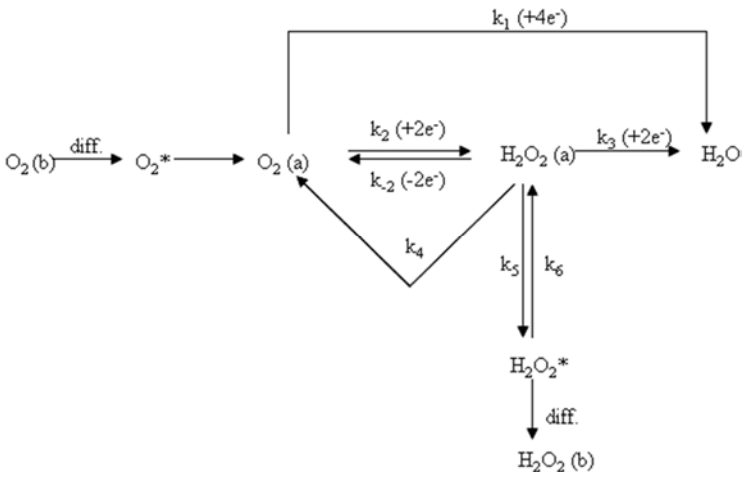

Figure 4.2 Reaction pathways proposed for the ORR given by Wroblowa *et al* [49].

In order to accelerate the ORR kinetics different catalysts have been tested; as known catalysts lower the activation energy by being the intermediate of the reaction. The most used catalyst till now is Pt, however, as known, Pt is expensive and scarce in nature, facts that limit its practicability on a large-scale. Today low-Pt, Pt-alloys, non-Pt, non-noble metal and even non-metal (organic) catalysts are being researched and developed.

4.2 ORR on Pt

It is proven that Pt has better activity towards ORR than other noble metals, they can be arranged as Pt > Pd > Ir > Rh. On the other side Pt combined with other metals, noble or non-noble, exhibits better performance than pure Pt [42].

Pt is favorable because of his short Pt-Pt interatomic distances, high d-band vacancies and surface roughness. Usually ORR on Pt proceeds via 2 mechanisms:

* represents an active site on Pt surface

1) Dissociative Mechanism

$$1/2O_2 + * \rightarrow O*$$

$$O* + H^+ + e \rightarrow OH* \qquad \text{Rate Determining Step}$$

$$OH* + H^+ + e \rightarrow H_2O + *$$

The above mechanism describes the 4 electron-pathway, Pt surface adsorbs O_2 and breaks the O-O resulting in formation of atomic O. The atomic O accepts protons from the electrolyte and electrons from the electric circuit, eventually scheming water.

2) Associative Mechanism

$O_2 + * \rightarrow O_2*$

$O_2 + H^+ + e \rightarrow HO_2*$ Rate Determining Step

$HO_2* + H^+ + e \rightarrow H_2O + O*$

$O* + H^+ + e \rightarrow OH*$

$OH* + H^+ + e \rightarrow H_2O + *$

This mechanism may proceed in 2 different directions depending on the formation, or not, of hydrogen peroxide (H_2O_2). H_2O_2 can be formed because O_2 is present on the Pt surface and may obstruct the breaking of O-O bond. If H_2O_2 is formed, it can be either reduced to water or, when strong adsorbents are present on the solution, be the final product itself [29].

Summarizing, the ORR on Pt is affected by the adsorption of O_2, the dissociation of O-O bond, the binding of OH on its surface, and on how easily these reactions can take place. The Pt d-band vacancy (electronic) and Pt-Pt interatomic distance (geometrical) are crucial parameters for the above reactions. So, it is reasonable when we say that Pt catalysts can be affected by the structure, the particle size or the shape [42]. Different steps and terraces , on the surface of Pt, largely affect the ORR; for instance studies have proven that in weakly adsorbed electrolytes, such as $HClO_4$, the activity towards ORR follows the order: Pt(110)>Pt(111)>Pt(100), where Pt is a single crystal [43]. This order is theoretical and can be changed, for example by surface reconstruction, due to different electrolyte or operating conditions. This reconstruction may lead to surface terraces that adsorb O species less strongly than before; terraces are believed to be where active sites are located. Generally, surfaces with higher number of edges, kinks and steps, even though they are constrained by their tendency to bind O_{ads} and OH_{ads} stronger, exhibit in fact higher ORR activity [46, 48].

Intermediate species such as OH_{ads}, O_{ads} and H_2O_2 can seriously affect the ORR activity. OH_{ads} and O_{ads} can occupy active sites of Pt, where O_2 is adsorbed, altering its overall ability to further adsorb O_2. These species can be identified during a CV in 3 different regions (see Fig. 4.3). High potential values lead to more OH_{ads} occupying sites and generation of more stable O_{ads} sites. On the contrary a small number of experiments indicate that this intermediate species coverage helped the ORR kinetics.

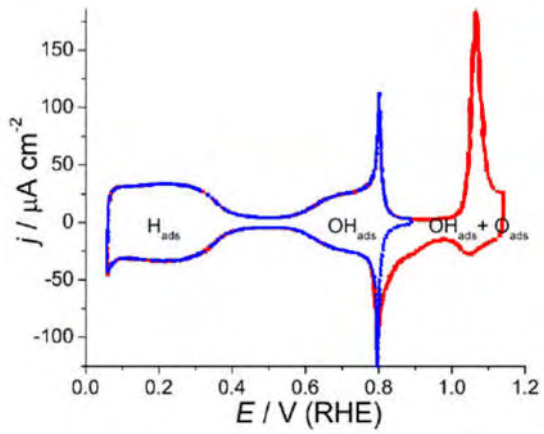

Figure 4.3 Presentation of ads-species areas during a cyclic voltammetry, for a Pt (1 1 1) electrode on HClO4 solution, with a a) 0.9V and b) 1.15V upper potential limit [45].

Studies showed that when H_2O_2 is present as an intermediate or as final product it causes a slow first electron step, resulting in ORR kinetics deterioration. H_2O_2 was observed on an electrode surface under the circumstances of high mass transfer or cases where anions were strongly adsorbed by the catalyst [46].

4.3 Pt alloys

Pure Pt exhibits high binding energy with oxygen species, this is a serious drawback leading to more condensed, of oxygen intermediates, surfaces. As a result, active sites that enhance the ORR are decreased.

According to Sabatier's principal, the preferred binding energy, of oxygen, is found to be about 0.2 eV weaker than Pt [29]. That proves that an electrocatalyst must not bind oxygen too strong neither too weak, because respectively it can't disassociate oxygen species, or the reaction won't occur at all. Pt combined with other metals, either noble (Ir, Pd, Rh, Ru, Au, Ag etc), either early transition metals (Cu, Fe, Ni, Co), can alleviate the precedent problem and even show further enhanced abilities and stability towards ORR, studies indicate an activity of 1.5-2 times superior compared with pure Pt [50].

This enhancement is linked to ligand effects (electronic charge transfer effects) changing the d-band vacancy, shortening of the Pt-Pt interatomic distances and increase of alloyed catalyst's surface due to alloyed metal dissolution [43]. That dissolution, caused by post treatment of the catalyst, leads to the formation of a pure Pt nano-porous surface layer, Fig. 4.4., called Pt skeleton or Pt skin, depending on the degree of coverage, which comprehends the properties of Pt. That phenomenon, leaching of transition metals and surface diffusion of Pt, happens only when the alloy particle size

overcomes a critical size. That nano-porous surface, created, binds oxygen more strongly, leading to higher surface area and subsequently more active sites, eventually improving ORR activity [48].

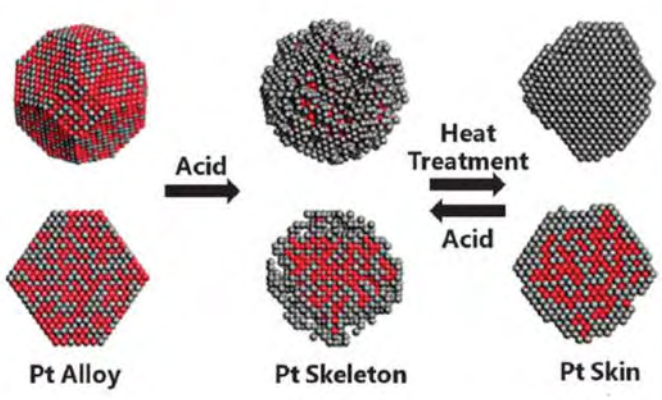

Figure 4.4. Illustration of the reversible formation of Pt Skeleton and Pt Skin, on a Pt alloy, for the stages of acidic and heat treatment [48].

Pt is often alloyed with other noble metals (Ir ,Pd ,Au ,Ag ,Ru etc.) ,as well as with first row transition metals (Cr .Mn ,Fe ,Co ,Ni etc.) , to exhibit the above-mentioned enhancements [51]. These alloys, according to Sabatier's principal, exhibit a 'volcano' type catalytic ability towards ORR, meaning their catalytic ability is getting better, by raising the analogy of the second metal towards Pt ,until a certain 'peak' is reached and then it starts deteriorating. In their top performance, some of these alloys, show Pt mass activity (mA/mg_{Pt}) several times bigger in contrast to pure Pt. In a Tafel slope, that enhancement can be illustrated by an improvement up to 50mV/dec in performance [50]. Carbon usually supports pure Pt and its alloys, because carbon possesses good electrical and mechanical properties alongside good adjustability of its pores size and distribution.

The best metals, to be alloyed with Pt, are considered being Co, Ni and Fe [52]. The fact that they are overabundant on earth's crust, cheaper compared to noble metals, alongside with their remarkable activities make them suitable for the ORR.

4.4 Other Metals

The previously mentioned metals have also been studied for Pt's replacement, as the main catalyst; however, none of them was as stable and kinetically efficient as Pt.

Pd the second most active catalyst, after Pt, has 5 times lower mass activity than Pt [53], and today is more expensive than Pt. Nevertheless, Pd can have its surface structure modified or can be alloyed with other metals and eventually reach Pt's activity. Pd price used to be 3 to 4 times lower than that of Pt; however, today Pd is

more expensive than Pt and for this reason not a viable option to serve as a catalyst for the ORR.

Metal chalcogenides have also been investigated for the ORR in a fuel cell because of their remarkable stability. Chalcogenides are chemical compounds consisted of one or more chalcogen elements, usually it is illustrated as M-X (where M=noble or transition metals, X=S, Se, Te). Among noble metals, Ru combined with Se seems to be the most promising catalyst, especially when Se added to Ru it improves its d-band distances (Ru atoms are be considered to be the active sites) making it comparable with Pt. However, Se toxicity must be taken in mind for future research and development on these catalysts. Transition metals have also been researched because of their price and abundance, Co was distinguished in particular combined with S, although its activity was pretty smaller than Ru_xSe_y. Chalcogenide's further performance enhancement is being tested with the addition of high conductive supports or of another chemical element (ternary) [44, 48].

Nitrogen-doped Carbon-supported Metal catalysts (M-N-C) are usually made from pyrolysis of transition metals precursors, leading to nitrogen precursors being adsorbed into carbon supports. These electrocatalysts are under research, in alkaline electrolytes, for their low price, high electrocatalytic activity, their great stability and tolerance to methanol crossover effect [54]. Doping with nitrogen during pyrolysis leads to formation of a carbon catalytic layer, meaning more active sites weakening the O-O interatomic bond. N_4 macrocycles, inorganic N (ammonia), organic molecules and N-containing polymers are commonly used as N precursors. Nevertheless, much more effort and research are needed, in order the M-N-C catalysts reach the activity of Pt/C. Some factors that govern their improvement are: i) how active sites can be affected from the interactions and composition of the different elements involved, ii) how pyrolysis affects the surface and structure of the catalyst, thus affecting the accessibility, into the active sites, of the oxygen species [48].

4.5 Metal-Free

The most well-known catalysts on this category, owed to their remarkable durability and methanol crossover tolerance, are the ones made of carbon materials, such as grapheme, carbon nanotubes, graphite, glassy carbon, active carbon etc. The way ORR mechanism is catalyzed differs between the previous mentioned carbon-

based materials, among them the most researched are carbon nanotubes (CN) and carbon doped by heteroatoms [55].

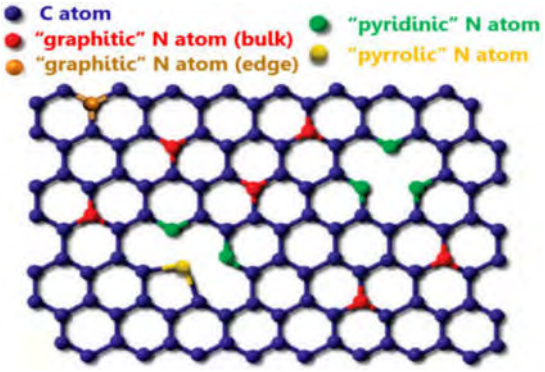

Figure 4.5 Schematic demonstration of a N-doped graphene sheet [56].

Carbon nanotubes ORR activity is highly dependent from their preparation method, but this field is not yet fully understood and further investigation must be made. Traditional CN catalyze ORR better on alkaline solutions; in order to enhance their activity on acid electrolytes, experiments were conducted trying to boost the number of CN active sites by changing its structure and formation [54]. These changes though, could degrade the excellent electrical conductivity and corrosion resistance that CN already exhibit [57].

Heteroatom doped carbon is a more researched field, especially for Nitrogen doped (N-doped) carbon. Other investigated heteroatoms are B, S, Se, P and F, they very often combined together making dual doped carbon catalysts and so on. N-doped carbon materials exhibit N-sites, on their surface or even inside their structure, which are accused for the improvement of ORR activity among other parameters, like carbon edge sites, surface area and N content [58]. These N-sites can be distinguished between pyridinic, pyrrolic and graphitic N atoms; they usually are uniformly distributed and it's not yet clear who has the bigger role on enhancing the ORR activity. N doping it's not only enhancing the ORR by reducing oxygen better but also by the decomposition of the H_2O_2 intermediates [59].

Even though they are often referred as 'Metal Free' catalysts, these carbon materials usually involve some metal traces, found either as impurities inside the material (graphite) or they can be introduced by metal precursors used during the preparation (N doped) of the catalyst. The impact of these metal traces is so strong that, even around 10-100 ppm of metal inside the catalyst, can produce a change of 80 mV on over-potential, an indication of how strongly ORR is affected by these traces [48].

CHAPTER V

ELECTROCHEMICAL TECHNIQUIES & BASIC ELECTROCHEMISTRY

5.1 Conventional Three-Electrode Cell

The most of electrochemical characterization experiments are conducted in an experimental configuration, which consists of an electrochemical cell with three electrodes, a working (W), a counter or auxiliary (C) and a reference electrode (R), all immersed in a solution and connected to a potentiostat. The potentiostat controls the potential difference between the working and the reference electrode, which is the potential of interest, with minimal interference from ohmic drop. Moreover, the potentiostat has a high input impedance, so that the current of the reference electrode is kept at a negligible value, therefore the potential difference between the reference and the working electrode to be maintained stable [60]. In Fig. 5.1 a three-electrode cell and a three-electrode potentiostat system are shown.

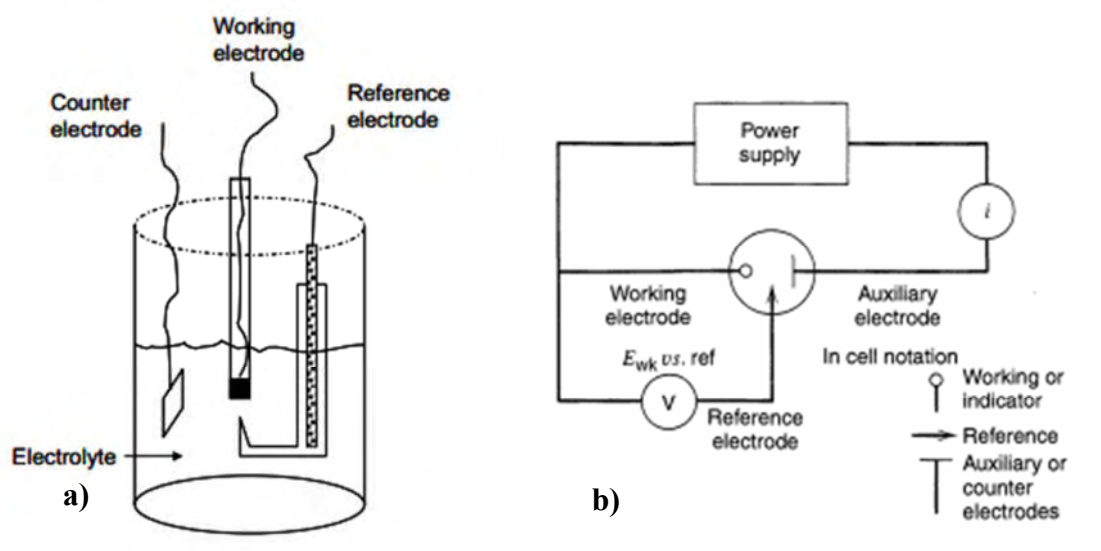

Figure 0.1 a) a conventional three-electrode cell [29] and b) three-electrode potentiostat system [8].

As it is depicted in Fig. 5.1b. the working and the counter electrode form a circuit where the current of interest passes through it, in response to the constant potential

difference between the working and the reference electrode. The counter electrode should be a non-reactive electrode with high surface area, usually a platinum gauze, in order not to interfere with the working electrode [60]. Note that the circuit between the working and the reference electrode contributes to minimizing the impact of the electrolyte resistance on the potential of the working electrode. Modifying the electronic circuit in such a way as to control the current and measure the potential of the working electrode, leads to a galvanostat [29].

5.2 Cyclic Voltammetry

Cyclic voltammetry (CV), a sweep reversal method, is among the most widely used of all the electrochemical methods for obtaining information about complicated electrode reactions. CV can be applied to obtain mechanistic, analytical, thermodynamic and kinetic information about chemical systems in which redox chemistry plays role [60]. Cyclic voltammetry refers to cycling the potential between a high and a low potential value and measuring the current in the potential cycling region. The potential is swept linearly with a constant sweeping rate. The scanning rate in most studies varies between 1 and 100 mV s^{-1}. The resulting potential versus current plot is called a voltammogram [61].

The behavior of the cell under CV experiment becomes clear by considering the influence of the potential on the equilibrium achieved at the electrode surface. If the rate of electron transfer is fast compared to the potential sweep rate, then at the electrode an equilibrium is established, which can be predicted by thermodynamics. Before the scanning starts, the working electrode is held at its initial potential, where no electrochemical reactions occur. After the scan is started, the voltage is swept from initial potential to the set potential and equilibrium position shifts from no conversion to full conversion of reactants at electrode surface. This situation is described well by Nernst equation [8]. In the case of reduction (or oxidation), the potential goes to lower values (or higher) and when the electrochemically active species are reduced (or oxidized) a cathodic (or anodic) current appears. The cathodic (or anodic) current increases as far as potential decreases (or increases) because the reaction kinetics becomes faster. At the reduction (or oxidation) potential of the analyte a current peak appears. While potential keeps sweeping, current decreases as the concentration of the analyte is depleted close to the electrode surface [29]. In Fig. 5.2 a typical cyclic

voltammogram with the characteristic parameters and a typical cyclic voltammetry waveform are shown.

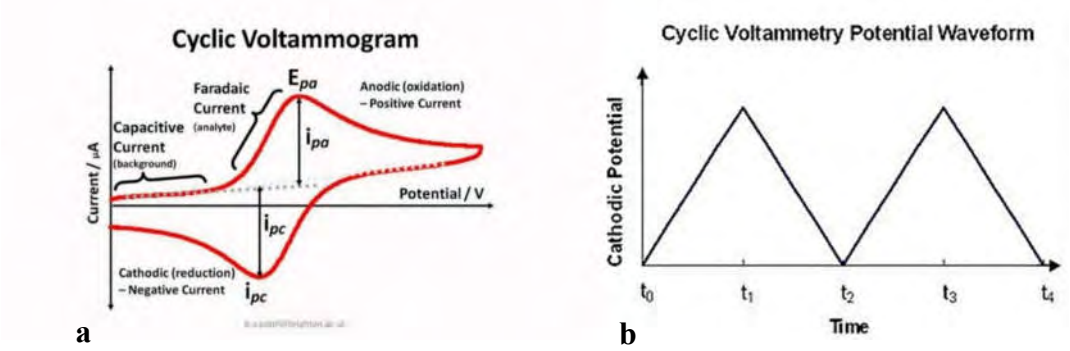

Figure 0.2 a) a typical cyclic voltammogram and b) voltammetry potential waveform [62].

The characteristic parameters of the cyclic voltammogram are presented below [61].

- E_{pa}, E_{pc}: anodic and cathodic peak potentials.
- i_{pa}, i_{pc} : anodic and cathodic peak currents. The positions of the peak currents do not change with the potential scan rate if the electrochemical reactions are reversible. In this case the peak current (anodic or cathodic) is given by the following equation:

$$ip = (2.69x10^5)n^{3/2}AD^{1/2}v^{1/2} \qquad (5.1)$$

  where i_p is the peak current (A), n is the overall electron transfer number, A is the geometric area of the electrode (cm^2), D is the diffusion coefficient of the analyte in the electrolyte (cm^2/s), v is the potential scan rate (V/s) and C is the bulk concentration of the analyte (mol/cm^3).
- Faradaic current: is the current generated by the oxidation or reduction of some chemical substance at the electrode.
- Capacitive current (non-faradaic current): is the current that does not involve any chemical reactions (charge transfer). It is related with the charging and discharging of the electrical double layer capacitance.

5.3 Rotating Disk Electrode

The reactants transfer to or from an electrode via diffusion, convection and migration. The migration occurs due to the influence of an electrical field, thus for solutions with an excess of a supporting electrolyte it can be neglected. Convection's impact is minimal, so diffusion which occurs due to concentration gradient is the dominant process of mass transport phenomena [29]. The mass transport rate can be increased when a forced

convection is introduced. That can be achieved with hydrodynamic methods, which assume that convection maintains the concentration of all species uniform and equal to the bulk values beyond a specific distance from the electrode surface, called diffusion layer. Therefore, in this case convection controls the thickness of the diffusion layer, and diffusion controls the transfer rate of the reactants through the diffusion layer [8].

The most convenient and widely used hydrodynamic electroanalytical technique is the rotating disk electrode (RDE). Convection is achieved by rotating the electrode at constant frequency with respect to the stagnant electrolyte. The spinning of the electrode drags the liquid at its surface and due to centrifugal force, the solution is spun away from the center of the electrode in a radial direction. There is still a diffusion layer, which thickness is depended on the angular velocity ω (s^{-1}) of the electrode, $\omega=2\pi f$ where f is the number of revolutions per second. The higher the angular velocity, the smaller the thickness of the diffusion layer [8]. However, the angular velocity should be in the range of values where the flow remains laminar and at the same time the hydrodynamic approaches of RDE theory continue to apply. In most studies the angular velocity ranges between 10 s^{-1} and 1000 s^{-1} or 100 rpm and 1000 rpm [63]. In Fig. 5.3 the working principle of RDE system is shown.

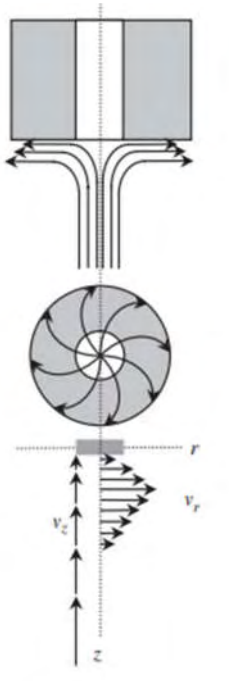

Figure 0.3 Streamlines for flow and vector representation of fluid velocities near a rotating disc electrode [61].

The rotating disk electrode technique is a linear sweep experiment in which the potential of the working electrode is swept from an initial potential, where no electrochemical reaction occurs, to a potential that causes an electrochemical reaction to occur. At a given electrode rotation rate, a limiting current appears when the reaction rate is determined by the mass transport rate. In this case the concentration of the reactants at the electrode surface drops at zero and a steady-state diffusion current is achieved [8]. This current is described by the Levich equation (5.2):

$$i_d = 0.62nFAD^{2/3}\omega^{1/2}\nu^{-1/6}C \quad (5.2)$$

where i_d is the limiting current under diffusion control (A cm^{-2}), A is the geometric area of the electrode (cm^2), n is the overall electron transfer number, F is the Faraday constant (96485 C/mol), D is the diffusion coefficient of the analyte in the electrolyte (cm^2/s), ω is the angular velocity (s^{-1}), ν is the kinematic viscosity of the electrolyte (cm^2/s) and C is the bulk concentration of the analyte (mol/cm^3). Before the achievement of the limiting current, the current is dominated both by the mass transport rate and the reaction kinetics. Right after the begging of the scanning (onset potential) the current is determined mainly by the reaction kinetics. In the entire potential sweeping region, the current is described by the Koutecky-Levich equation (5.3):

$$\frac{1}{i} = \frac{1}{i_k} + \frac{1}{i_d} \quad (5.3)$$

where i is the measured current, i_k is the kinetic current in the absence of mass transport effects and i_d the limiting diffusion current. A plot of i_k^{-1} and $\omega^{-1/2}$ at a given potential, is called Koutecky-Levich plot, which should be linear and for $\omega^{-1/2}=0$ i_k^{-1} is yield [61]. In Fig. 5.4 a typical linear sweep voltammetric measurement with RDE and a typical Koutecky-Levich plot are presented.

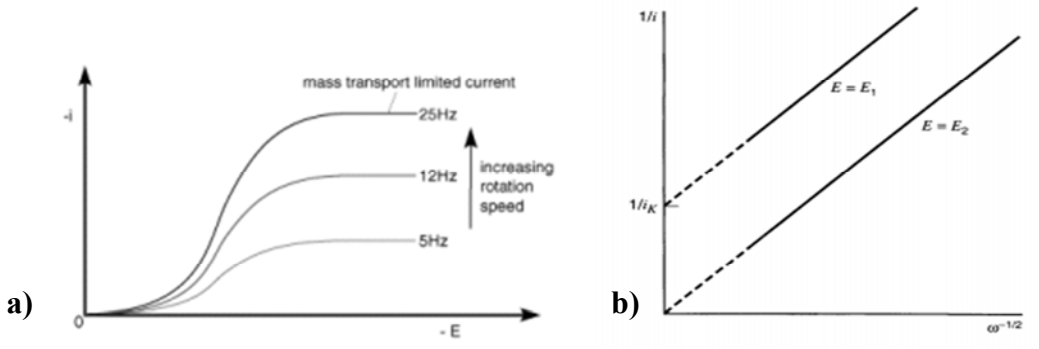

Figure 0.4 a) a linear sweep voltammetric measurement with RDE and b) a typical Koutecky-Levich plot [8].

5.4 Electrochemical Impedance Spectroscopy

Electrochemical impedance spectroscopy (EIS) is an electrochemical technique that presents the signal as a function of frequency at a constant potential. More precisely, a small-magnitude periodic electrical perturbation is applied to the electrochemical cell and its electrical response is measured at different frequencies [63].

The key step of EIS experiment is the construction of an equivalent electrical circuit that imitates the electrical behavior of the electrochemical cell. The components of the equivalent circuit represent the chemical or physical characteristics of the cell, and its overall configuration is related to the different ways that the ionic charges are involved in the passage of current [61]. In Fig. 5.5 the simplest electrical equivalent circuit is shown.

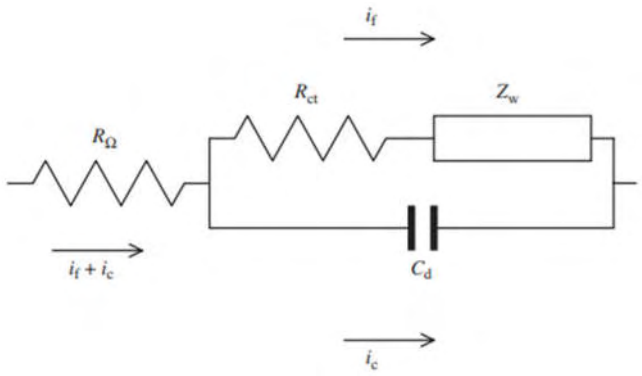

Figure 0.5 Equivalent electrical circuit for a simple reversible electron transfer [61].

The characteristic components of the circuit and their relation to the electrochemical cell are presented below [8].

- R_Ω (ohmic solution resistance): The solution between the electrodes behaves as an ionic conductor with a specific resistance. The value of the resistance depends on the conductivity of the solution, the distance between the electrode and the cross-sectional area of solution linking the electrodes.
- R_{ct} (charge transfer resistance): It represents the ratio of overpotential to current in absence of mass transport effects.
- Z_w (mass transport resistance): It depends on the mechanism of mass transport within the cell. For semi-infinite diffusion Z_w is a complex number.
- Combining Z_w and R_{ct} gives the faradaic impedance.
- C_d (double layer capacitance): It refers to the electrostatic interplay to the electrode-solution surface. It depends on the electrode area and the nature of the electrolyte.

- The combination of all the impedances gives the overall impedance of the cell which is a complex number.

$$Z_{cell} = Z_{Re} + jZ_{Im} \quad (5.4)$$

EIS data are represented in Nyquist and Bode plots. Nyquist diagram is resulted by plotting the real part of the impedance versus the imaginary part, and the Bode diagram by plotting the impedance magnitude and phase angle versus the frequency. Nyquist plot is the most usual way of presenting the impedance spectrum as it contributes to the extraction of several information, like R_Ω (from the high frequency intercept on the real axis), R_{ct} (from the diameter of the semicircle) and C_d (from the frequency at the maximum of the circle) [61]. A typical Nyquist plot with the key features is depicted in Fig. 5.6.

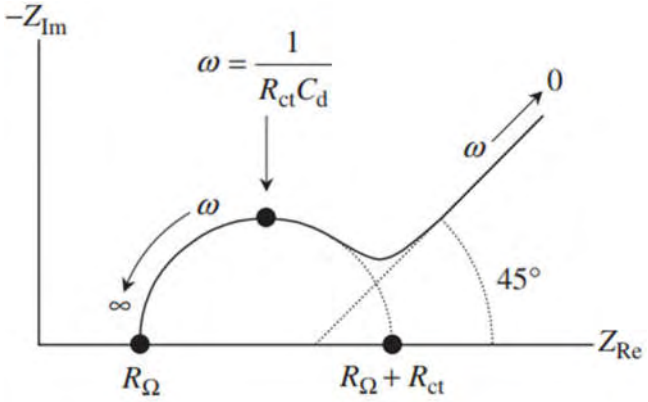

Figure 0.6. A typical Nyquist plot [61].

5.1 Thermodynamics

Gibbs free energy expresses the net-work obtained from the cell [8, 29].

$$\Delta Go = \Delta Ho \quad T\Delta So \quad (5.5)$$

where ΔH^o is the change of enthalpy and ΔS^o the change is entropy of the cell.

However, Gibbs free energy can be also be expressed as a matter of electrochemical quantities, for an electrochemical cell with an anode and a cathode we get,

$$\Delta G = nFE \quad (5.6)$$

n is the number of electrons involved in the cell reaction

F, the Faraday constant, equals 96485 Coulombs per mol

E or EMF is the electromotive force of the cell (inside an electrochemical cell it can be measured as the open-circuit potential).

If the substances inside the electrochemical cell act like a unit then we get another expression,

$$\Delta G^o = \quad nFE^o \tag{5.7}$$

E^o is called the standard electromotive force of the cell, and it's calculated for a pressure of 1atm and temperature of 25^{o}C.

Gibbs free energy is controlled by changes in pressure, temperature and concentration, so the overall change in free energy is calculated from,

$$\Delta G = \Delta G^o + RT\, ln \frac{a_{products}}{a_{reactants}} \tag{5.8}$$

where activity is symbolized with the letter a, and a=γc

γ is affected by the solution concentration and it's called activity coefficient

c is the well-known molar concentration [64].

According to convention, when ΔG is negative it means the cell is producing energy, positive means it consumes energy.

Now if we replace (5.6), (5.7) into (5.8), we get

$$E = E^o \qquad RT\, ln \frac{a_{products}}{a_{reactants}} \tag{5.9}$$

this relation is known as the Nernst equation, and helps us to associate cell potential with the activities, or concentrations, of the substances involved.

In order the above equations to apply; we need the cell to be as chemically, as thermodynamically reversible, meaning the cell reaction can take place in the opposite direction, without new reactions occurring.

5.2 Kinetics

Electrochemical equilibrium is where the net current equals zero, meaning that the two reactions are simultaneously taking place but with opposite directions and with the same speed. The rate that a simple reaction is processing can be expressed as,

$u_{net} = k_f C_{reactants} - k_b C_{products,}$

u_{net} [=mol s^{-1}]

k_f and k_b are rate constants with units s^{-1}

According to Faraday's law the current density equals,

$$i = nFu_{net} = nF(k_f C_{reactants} \qquad k_b C_{products}) \tag{5.10}$$

at equilibrium we acquire the so-called exchange current density i_o,

$$i_o = nFk_f C_{reactants} = nFk_f C_{products} \quad (5.11)$$

Arrhenius Equation manages to show the dependence of rate constants with temperature and activation energy,

$$k = Ae^{\frac{-E_A}{RT}} \quad (5.12)$$

where A is the frequency factor, and E_A is the activation energy.

The Arrhenius equation (5.12) can be associated with Gibbs free energy as,

$$k = \frac{k_B T}{h} \; exp\left[\frac{-\Delta G}{RT}\right] \quad (5.13)$$

k_B and h are the Boltzmann and Plank constants, respectively.

Now if we assume that we got an electrochemical cell where oxidation and reduction is taking place at different electrodes, we get

$$k_f = k^o \, e^{\left[\frac{-a_{Rd} nFE}{RT}\right]} \quad (5.14)$$

$$k_b = k^o e^{\left[\frac{a_{Ox} nFE}{RT}\right]} \quad (5.15)$$

k^o is called standard rate constant

Replacing (5.14) and (5.15) into current density equations (5.10) & (5.11),

$$i = nF\left[k_f C_{Ox} \, e^{\left[\frac{-a_{Rd} nFE}{RT}\right]} - k_b C_{Rd} \, e^{\left[\frac{a_{Ox} nFE}{RT}\right]}\right] \quad (5.6)$$

$$i_o = nFk^o C_{Ox,eq} \, e^{\left[\frac{-a_{Rd} nFE_{eq}}{RT}\right]} = nFk^o C_{Rd,eq} \, e^{\left[\frac{a_{Ox} nFE_{eq}}{RT}\right]} \quad (5.17)$$

For the transfer coefficient, a, it applies that $a_{Rd}+a_{Ox}=1$,

$E-E_{eq}=\eta$, where η is the overpotential,

and by assuming $C_{Ox}=C_{Ox,eq}$ & $C_{Rd}=C_{Rd,eq}$,we finally get

$$i = i_o\left[e^{\frac{a_{Rd} nF\eta}{RT}} \quad e^{\frac{(1-a_{Rd})nF\eta}{RT}}\right] \quad (5.18)$$

Equation (5.18) is known broadly as the Butler-Volmer formulation, and it links the current with the overpotential of an electrochemical cell. This equation can be applied only when the rate determining step is not mass transfer.

For low overpotential the equation (5.18) can be simplified to,

$$i = i_o \frac{nF\eta}{RT} \quad (5.19)$$

For high overpotential, one term of Butler-Volmer equation can be eliminated, depending if we overpotential is positive or negative, so we have

$$i = i_o e^{\frac{-anF\eta}{RT}} \quad \text{or} \quad i = i_o e^{\frac{(1-a)nF\eta}{RT}} \tag{5.20}$$

in order to make things simpler a_{Rd} is written as a.

By solving these 2 equations (5.20) for the overpotential η, we get

$$\eta = \frac{RT}{anF} lni_o \quad \frac{RT}{anF} lni \tag{5.21}$$

here we dictate 2 parameters a and b, where

$a = \frac{2.3\,RT}{anF} logi_o$ & $b = \frac{2.3\,RT}{anF}$, and finally, we get

$$\eta = a + blogi \tag{5.22}$$

This equation (5.22) is called Tafel equation and by plotting overpotential with current density, on a logarithmic scale, we get the Tafel Slope (Fig. 5.7). The higher the slope's inclination, the slower kinetics of the reaction .This can be explained by thinking that, for high slope's inclinations the overpotential increases faster as the current density increases. The desired reaction is one where current density increases fast while overpotential change is small. The Tafel slope is affected by the transfer coefficient (a), and the number of electrons involved (n).

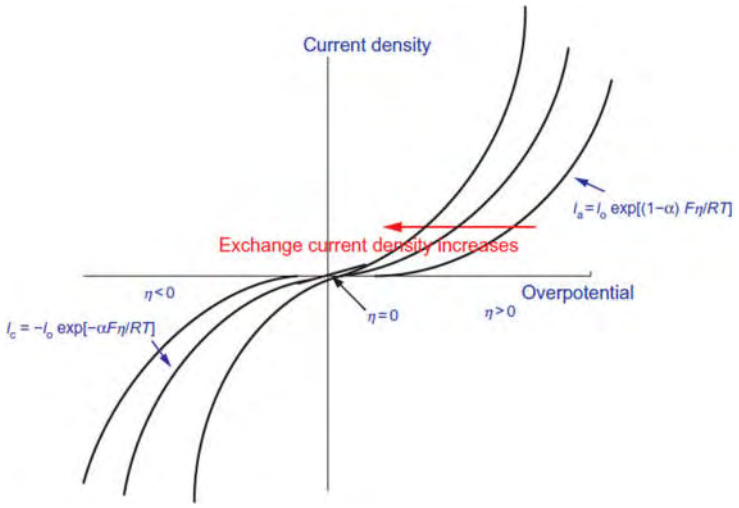

Figure 0.7 Tafel plots affected by exchange current density (io) and transfer coefficient (a) [65].

The transfer coefficient is largely dependent from temperature and for the oxygen reduction reaction it can be written as,

a=0.01678*T, T in Kelvin degrees [29].

CHAPTER VI

EXPERIMENTAL PART

6.1 Electrochemical Characterization

All electrochemical measurements were carried out with an electrochemical workstation AMEL 7050 in a three-electrode cell, employed with a Pt wire and a saturated calomel electrode (SCE) as counter and reference electrodes, respectively. A glassy carbon (GC) disk electrode was used as a working electrode (diameter 3.0 mm, A_{geo}=0.07 cm^2), mounted on an RDE holder, on which the thin film of the selected electrocatalyst was deposited.

All electrochemical measurements were conducted in 0.1 M $HClO_4$ aqueous solution at room temperature. The catalyst total loading, for all measurements and all electrocatalysts used, was maintained 71.43 μg cm^{-2}. All potentials presented are quoted versus a reversible hydrogen electrode (RHE) as it is described by the following equation:

$$E(RHE) = E(SCE) + 0.241 + 0.059pH \quad (6.1)$$

with pH=1 for 0.1 M $HClO_4$ aqueous solution

6.1.1 Preparation of the electrocatalytic ink

The tested electrocatalysts are Pt, Pd, Ir, Pt_xIr_y and Pt_xPd_y (with x:y atomic ratios 3:1, 1:1, 1:3), all with 20 wt% metal loading and supported on Vulcan XC-72. The electrocatalytic ink was prepared with the same way for each electrocatalyst used. More precisely, the electrocatalytic ink was composed of 5 mg of the selected electrocatalyst powder, 1.7 mL deionized water, 0.3 mL propanol (C_3H_8O) and 10 μL of 5 wt% Nafion solution. The suspension was sonicated in an ice bath, placed in the ultrasonicator for 30 minutes, to obtain a well-dispersed ink. 10 μL of the as-prepared ink was pipetted onto the surfaces of the GC electrodes, which previously were cleaned via polishing with a deionized water-alumina slurry. After the polishing, the electrodes were sonicated in the ultrasonicator for 10 minutes. Then the GC electrode

was placed on an inverted rotator shaft and rotated gradually increased from 400 to 500 rpm for an hour, for the purpose of drying the electrocatalytic thin film.

6.1.2 Cyclic Voltammetry (CV)

Before each experiment the solution was saturated with high-purity N_2 gas for 30 min in order to remove the dissolved oxygen in the electrolyte. First the electrodes were conditioned by CV under N_2- saturated solution for 30 min (75 cycles) from 0.15 to 1.25 V vs RHE at 100 mV s^{-1}. After the electrode conditioning procedure, a cyclic voltammogram was conducted at 50 mV s^{-1} from which the electrochemical active surface area (ECSA) was calculated.

6.1.3 Linear sweep voltammetry (LSV) with the aid of RDE

In order to impose LSV to characterize the selected catalysts in terms of their electrocatalytic activity, O_2 gas was supplied to the electrolyte for 30 min until a saturated solution was created. LSV was conducted at 20 mV s^{-1} with anodic sweep for every experiment.

The LSVs which are presented at the following chapter have been corrected for background currents and solution resistance in order to obtain more accurate results for the kinetic behavior of the electrocatalysts. The background currents correction was accomplished by subtracting the LSV curves obtained under O_2 and N_2 with identical experimental parameters. This correction leads to results that are independent of the capacitive currents and Faradaic currents associated with hydrogen adsorption/desorption and oxide formation/reduction processes.

6.1.4 Resistance measurement and Electrochemical Impedance Spectroscopy (EIS)

Before the beginning of each electrochemical measurement the resistance of the solution was measured with the aid of electrochemical impedance spectroscopy (EIS). More precisely, the magnitude of the solution resistance was obtained by the real intercept of the Nyquist plots with frequency range from 10 kHz to 0.02 Hz, at 0.8 V vs RHE. In order the experiments to start the $R_{solution}$ should be lower than 10 Ohm.

CHAPTER VII

RESULTS & DISCUSSION

7.1 ORR electrocatalytic activity over Ir, Pt and Pt_xIr_y supported on Carbon (Vulcan XC-72)

7.1.1 Cyclic voltammetry and electrodes conditioning results

The cyclic voltammograms, before and after the electrodes conditioning procedure for each electrocatalyst, are shown in Fig. 7.1. The electrodes were conditioned under N_2-saturated 0.1 M $HClO_4$ aqueous solution for 30 min (75 cycles) at 100 mV s^{-1}.

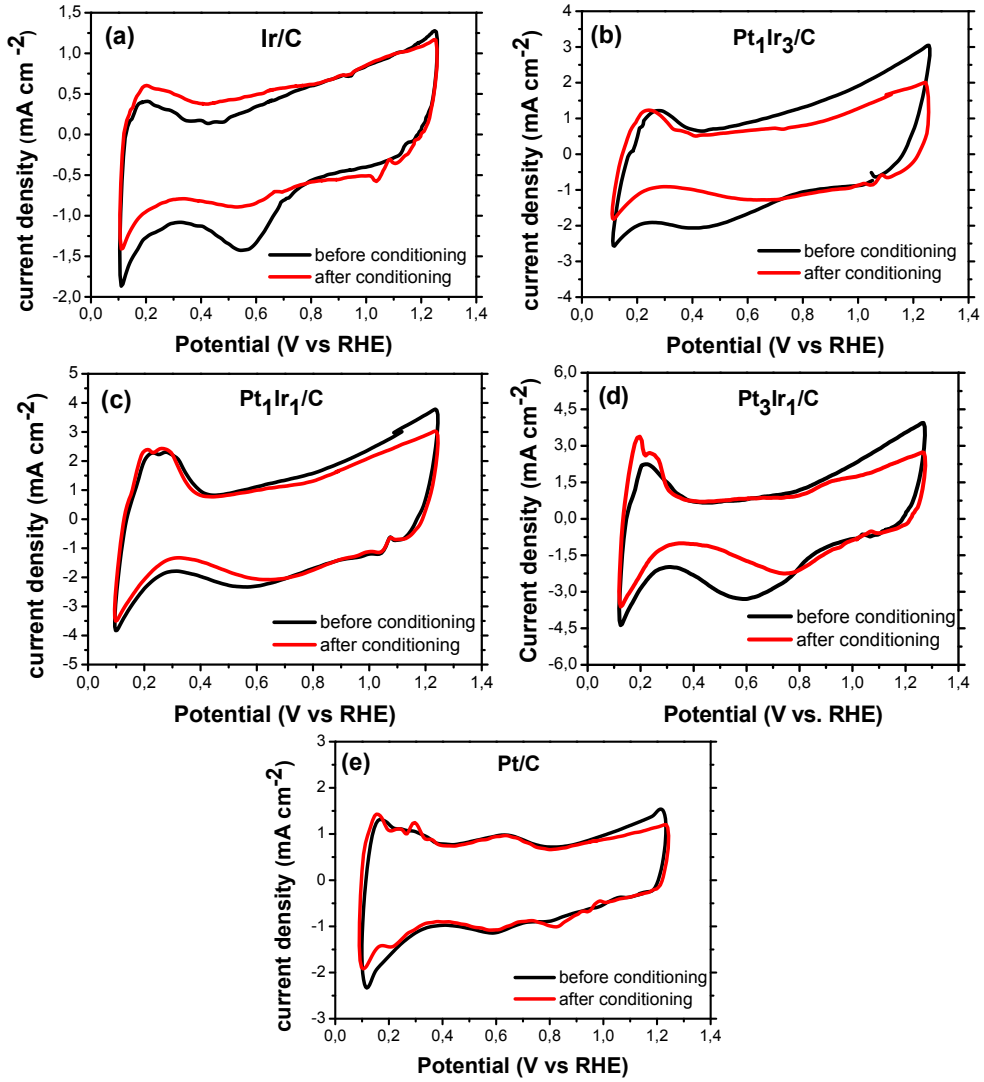

Figure 7.1 CV curves before and after conditioning in N_2-saturated 0.1 M $HClO_4$ aqueous solution, at a scan rate of 50 mV s^{-1} for a) Ir/C, b) Pt_1Ir_3/C, c) Pt_1Ir_1/C, d) Pt_3Ir_1/C and e) Pt/C (20 wt%).

The electrodes conditioning procedure contributes to the oxidation/removing of the adsorbed oxygen and other impurities from the electrode's surfaces, and to the formation of a stable re-organized surface, leading to the conduction of reproducible experiments. In conclusion, the conditioning procedure contributes to peak ECSA and ORR activity results [66].

From Fig. 7.1 it can be seen that the area of the double layer charging region (0.4 to 0.6 V vs RHE) decreased after the conditioning procedure, indicating that the charging of the double layer was accelerated. Furthermore, the surface oxide formation region (0.6 to 1.25 V vs RHE) shifted to lower current values. Also, the oxide reduction region and peak shifted to more positive potentials. These modifications to the CV curves after the conditioning procedure indicate that the mass transport rate was increased, hence also the electrocatalytic activity. Finally, the hydrogen adsorption and desorption peaks shifted in such a way that the ECSA increased after the conditioning process.

According to the above analysis and the moderate ECSA of Pt, it can be noted that the Pt catalyst (Fig. 7.1e.), exhibits the least impact among the tested electrocatalysts in the conditioning procedure, fact which may be explained from its tendency to associate oxides strongly [42]. These conclusions confirm that the absorbed oxygen and the impurities on the surfaces of the electrodes adversely affect their ORR activity.

The cyclic voltammograms of Pt, Ir and Pt_xIr_y supported on Vulcan XC-72, conducted in N_2-saturated 0.1 M $HClO_4$ aqueous solution at 50 mV s^{-1}, are shown in Fig. 7.2.

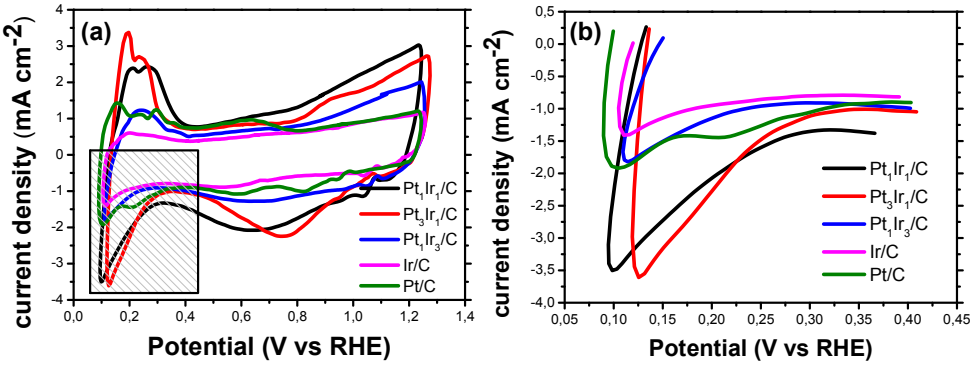

Figure 7.2 a) CV curves in N_2-saturated 0.1 M $HClO_4$ aqueous solution, at 50 mV s^{-1} and b) hydrogen adsorption peaks.

From the cyclic voltammograms presented on Fig. 7.2 it can be seen that the hydrogen adsorption and desorption region appear, for all the tested catalysts, at potentials below 0.4 V vs RHE, the double layer charging region from 0.4 to 0.6 V vs RHE and the surface oxide formation region from 0.6 V to 1.25 V vs RHE. The onset

potential for the surface oxide reduction in the cathodic scan appears, approximately for all the tested electrocatalysts, at 1.0 V vs RHE.

The electrochemical active surface area (ECSA) values were evaluated from the surface integration of the hydrogen adsorption peak taken by the cyclic voltammogram, calculated according to equation 7.1.

$$ECSA\ (\frac{cm^2}{\mu g}) = \frac{Q_{H,ads}}{M_{load}\ (X_{Pt}Q_{Pt}+X_{Ir}Q_{Ir})} \quad (7.1)$$

where $Q_{H,ads}$ (μC cm^{-2}) is the integrated charge on the hydrogen adsorption peak, M_{load} is the metal loading on the working electrode's surface (71.43 μg cm^{-2} for all the tested electrocatalysts), Q_{pt} =210 μC cm^{-2} and Q_{Ir} =218 μC cm^{-2} are the charges due to oxidation of a monolayer of adsorbed hydrogen per unit area, and X_{Pt}, X_{Ir} are the atomic fractions of the metals on the alloy surface [67]. The estimated ECSA for the tested electrocatalysts are presented on Table 7.1.

Table 7.1 Estimated electrochemical active surface areas.

Electrocatalyst (20 wt% metal loading)	**ECSA ($m^2\ g_{PGM}^{-1}$)**
Pt_1Ir_1/Vulcan XC-72	27.5
Pt_3Ir_1/ Vulcan XC-72	30.4
Pt_1Ir_3/ Vulcan XC-72	10.4
Ir/ Vulcan XC-72	6.70
Pt/ Vulcan XC-72	15.3

It is found that Pt_3Ir_1 displays the highest ECSA value (30.4 $m^2\ g^{-1}$) among the tested electrocatalysts, followed in sequence by Pt_1Ir_1, Pt, Pt_1Ir_3 and Ir. According to these results it can be said that iridium, at a higher loading percentage than platinum in Pt_xIr_y bimetallic catalysts, contributes to the decrease of the ECSA, compared to that of Pt. Note that the electrochemical active surface area determines the electrocatalytic activity, as it expresses the surface active centers of the electrocatalyst, in which the catalytic processes occur [67].

7.1.2 Oxygen Reduction Reaction (ORR) Kinetics

The ORR activity of the tested electrocatalysts was examined by rotating disk electrode (RDE) experiments, from which the corresponding linear sweep voltammetry (LSV) curves were taken. All RDE experiments were conducted under O_2-saturated 0.1 M $HClO_4$ aqueous solution, at a scan rate of 20 mV s^{-1}, at rotation rates from 400 rpm to 2000 rpm.

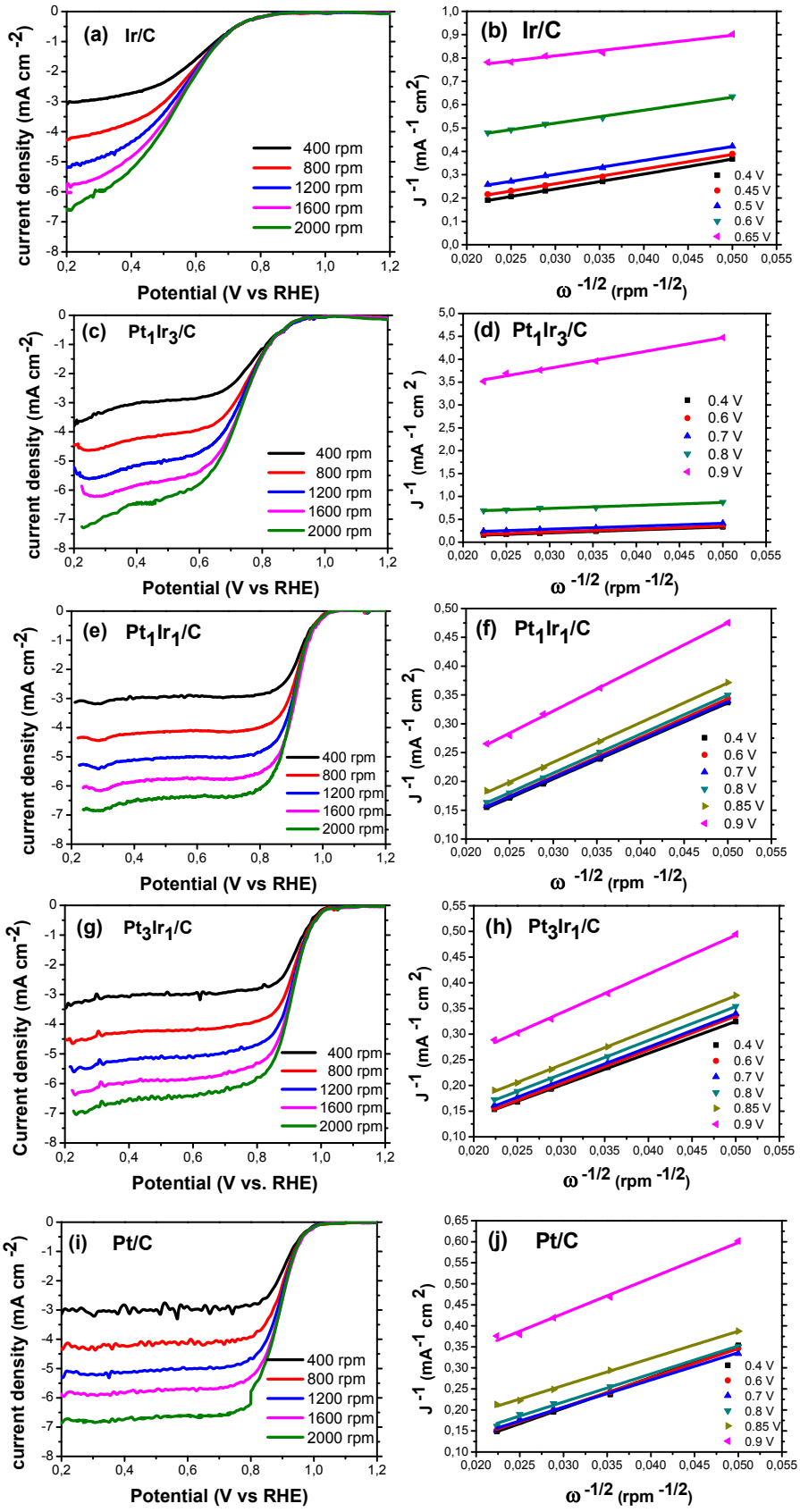

Figure 7.3 LSV curves in O_2-saturated 0.1 M $HClO_4$ aqueous solution, at rotation rates from 400 to 2000 rpm, at a scan rate of 20 mV s^{-1} for a) Ir/C, c) Pt_1Ir_3/C, e) Pt_1Ir_1/C, g) Pt_3Ir_1/C and i) Pt/C (20 wt%) and Koutecky-Levich plots for b) Ir/C, d) Pt_1Ir_3/C, f) Pt_1Ir_1/C, h) Pt_3Ir_1/C and j) Pt/C (20 wt%).

At first glance, from Fig. 7.3a. it can be clearly seen that Ir presents the lowest ORR activity among the tested electrocatalysts, as it exhibits the less positive onset potential. Furthermore, Ir is unstable as it does not display a flat plateau at the mass transport control region. Pt_1Ir_3 exhibits better ORR activity than Ir, however its onset potential is low compared to the other examined electrocatalysts. Pt_1Ir_1, Pt_3Ir_1 and pure Pt display similar LSV curves with high ORR activity, according to their onset potentials, their limiting currents and their half wave potentials, which are the potentials where the values of the currents are the half of the limiting currents.

Three different regions are displayed in each LSV curve: i) the kinetic control region (from 0.9 to 1.05 V vs RHE), where the current is dominated by reaction kinetics and it is independent of the rotation rate, ii) the mixed-control region (from 0.9 to 0.75 V vs RHE), where the current is controlled by both reaction kinetics and mass transport processes and iii) the diffusion control region at potentials below 0.75 V vs RHE, where the current is controlled by the rate of O_2 diffusion from the bulk solution to the catalyst-electrode surface [8].

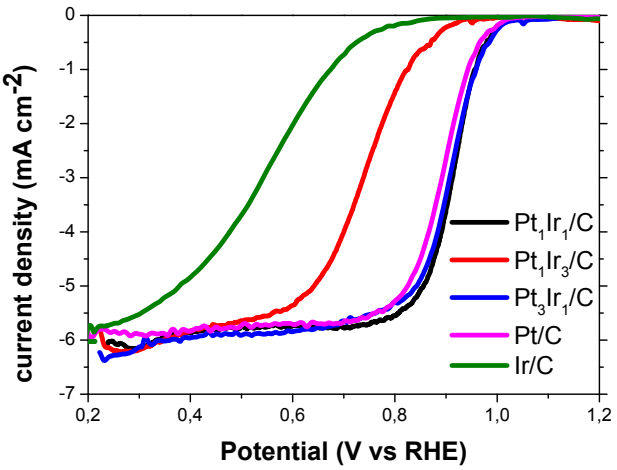

Figure 7.4 LSV curves in O_2-saturated 0.1 M $HClO_4$ aqueous solution, at 20 mV s^{-1}, at 1600 rpm.

The comparison between the electrocatalysts becomes clearer in Fig. 7.4, where the LSV curves at 1600 rpm are presented. The extracted results from the LSVs, at 1600 rpm, are summarized on Table 7.2.

Table 7.2 LSV properties for ORR at 1600 rpm.

Electrocatalyst (20 wt% metal loading)	**Limiting current (mA cm^{-2})**	**E_{onset} (V vs RHE) @0.1 mA cm^{-2}**	**$E_{1/2}$ (V vs RHE)**
Pt_1Ir_1/Vulcan XC-72	5.85	1.01	0.91
Pt_3Ir_1/Vulcan XC-72	5.96	1.03	0.91
Pt_1Ir_3/Vulcan XC-72	5.97	0.93	0.74
Ir/Vulcan XC-72	5.69	0.84	0.55
Pt/Vulcan XC-72	5.83	1.02	0.90

In order to examine the electrocatalytic activity for ORR more analytically, the kinetic parameters should be determined by the Koutecky-Levich equation (7.2). More precisely, from the intercept of the Koutecky-Levich plot for $\omega^{-1/2} \rightarrow 0$, shown in Fig. 7.3, the kinetic current density is emerged at a specific potential value, and from the slope, by using the Levich equation (7.3), the number of electrons transferred per oxygen molecule for oxygen reduction is calculated [68].

$$\frac{1}{i} = \frac{1}{i_k} + \frac{1}{i_d} \tag{7.2}$$

where i is the measured current, i_k is the kinetic current in the absence of mass transport effects, and i_d the limiting diffusion current.

$$i_d = 0.201 n F A D^{2/3} \omega^{1/2} \nu^{-1/6} C \tag{7.3}$$

where i_d is the limiting current under diffusion control (A cm^{-2}), A is the geometric area of the electrode (0.07 cm^2), n is the number of electrons transferred per oxygen molecule for oxygen reduction, F is the Faraday constant (96485 C/mol), D is the diffusion coefficient of O_2 in 0.1 M $HClO_4$ (1.9×10^{-5} cm^2/s), ω is the revolution rate (rpm/60), ν is the kinematic viscosity of the electrolyte (0.01 cm^2/s) and C is the O_2 concentration in 0.1 M $HClO_4$ (13.8×10^{-7} mol/cm^3) [66].

As it is shown in Fig. 7.3 (d., f., h. and j.), the Koutecky-Levich plots in each potential are linear and parallel for the most electrocatalysts, which indicates a direct 4-electron reduction pathway from O_2 to H_2O [68]. Indeed, the calculated number of electrons transferred is close to four for all the examined electrocatalysts (Fig. 7.5a.) and in the whole range of potentials. The only exception is Ir, which does not display linear Koutecky-Levich plots at high potentials, due to its instability, so no reliably results can be derived. In fuel cell processes, the direct 4-electron ORR pathway is desirable, as it contributes to maintaining the stability of the catalyst [29].

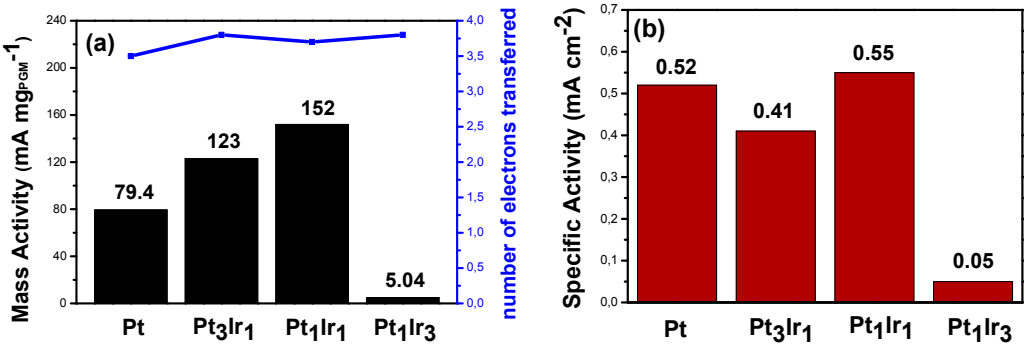

Figure 7.5 a) Mass activities and number of electrons transferred and b) specific activities at 0.9 V vs RHE.

As it is mentioned, the kinetic currents were emerged by the intercept of the Koutecky-Levich fitted straight lines for $\omega^{-1/2} \rightarrow 0$ [61]. The comparison between the electrocatalysts made at 0.9 V vs RHE. In the literature, it is customary to express the ORR activity in terms of mass activity (MA) and specific activity (SA), which are the kinetic currents per metal loading and per electrochemical active surface area, respectively. The kinetic current density corresponds to the intrinsic activity of the catalyst [8], so according to the results from the Koutecky-Levich analysis presented in Fig. 7.5, it can be deduced that Pt_xIr_y catalysts with Ir loading percentage 50% or less contribute to the enhancement of the ORR activity compared to Pt catalyst.

From Fig. 7.6, it can be clearly observed the ‘‘Volcano’’ type dependency of mass and specific activities in the Pt_xIr_y bimetallic catalysts. Finally, it is worth noting, that in the case of Pt catalyst, the moderate values of kinetic current density and ECSA, results in a remarkably high specific activity, (Fig.7.5b.), indicating the high electrocatalytic activity of platinum for ORR.

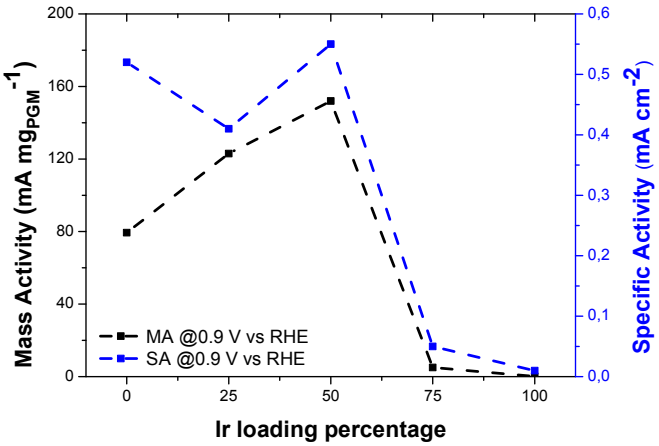

Figure 7.6 Mass activity and specific activity at 0.9 V vs RHE vs Ir loading percentage for ORR.

The electrocatalytic activity for the ORR can be further examined by the evaluation of the kinetic parameters derived from the analysis of the Tafel equation (7.4). These parameters are the exchange current density (i_0) and the Tafel slope at low overpotentials.

$$\log(i_k) = \log(i_0) \quad (\frac{\alpha n F}{2.303 RT})\eta \qquad (7.4)$$

where $i_k = \frac{i \, x \, i_d}{i_d - i}$ is the kinetic current density (mA cm^{-2}) derived from the Koutecky-Levich equation, i_0 is the exchange current density (mA cm^{-2}), α is the transfer coefficient, F is the Faraday constant (96485 C/mol), R is the gas constant (8.314 J mol^{-1}K^{-1}), T is the temperature (298 K), n the number of electrons transferred, and η is the overpotential (V vs RHE) [68].

The Tafel plots at low overpotentials for the examined electrocatalysts are shown in Fig. 7.7. As it was expected, based on the mass and specific activities extracted above, Pt_1Ir_3 shows up the highest Tafel slope among the tested electrocatalysts. On the other hand, Pt_1Ir_1 and Pt_3Ir_1 display the lower Tafel slopes (~65 mV/dec) with the Pt to follow the sequence with a slightly higher slope (71.8 mV/dec). According to these data and knowing that low values of Tafel slopes are desirable, since the smaller the slope, the less the overpotential increases with the current density, it is indicated that Pt_1Ir_1 and Pt_3Ir_1 represent the higher electrocatalytic ORR activity and by the same reasoning Pt_1Ir_3 the lowest. Moreover, these conclusions are confirmed by the determination of the exchange current densities, by the intercept of the linear Tafel plots for zero overpotentials. The exchange current density is proportional to the electrochemical reaction rate, thus the higher the exchange current density the higher the ORR electrocatalytic activity [8]. Pt_1Ir_1, Pt_3Ir_1 and Pt display similar values of exchange current densities, while Pt_1Ir_3 shows up the lowest value.

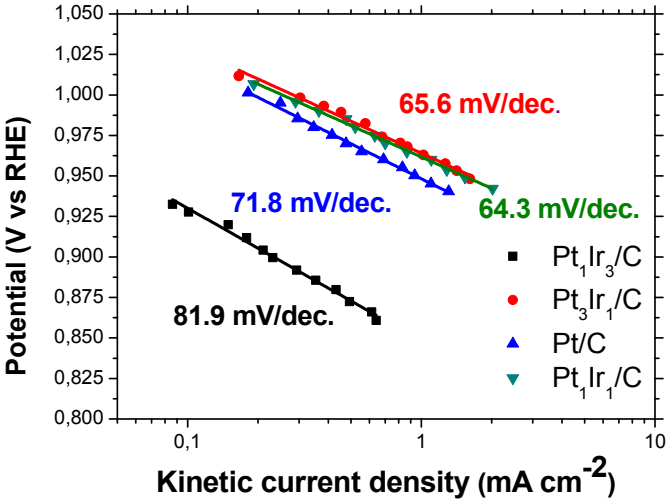

Figure 7.7 Tafel plots at low overpotentials.

According to Koutecky-Levich and Tafel results, for pure Pt and Pt_xIr_y catalysts, it is concluded that Ir in a metal loading percentage less than or equal to 50% at the bimetallic catalysts, contributes to the enhancement of the ORR electrocatalytic activity, compared to that of Pt. More precisely, Pt_1Ir_1 was found to be, among the examined electrocatalysts, the most favorable for the oxygen reduction reaction, according to its mass and specific activity, as well as its Tafel slope. According to the literature [69, 70] the enhanced ORR activity of Pt_xIr_y bimetallic catalysts is explained by the increase of the Pt 5d-vacancy and the positive binding energy shift of the Pt in the Pt-Ir alloy.

7.2 ORR Electrocatalytic activity over Pd, Pt and Pt_xPd_y supported on carbon (Vulcan XC-72)

In this chapter Pt_xPd_y bimetallic catalysts are characterized, as far it concerns their electrochemical properties and their suitability for the ORR. The electrochemical characterizations acquired are summarized in Table 7.3 and are further elaborated below.

Table 7.3 Electrochemical Kinetic properties of Pt, Pd, Pt_1Pd_3, Pt_1Pd_1 and Pt_3Pd_1.

Catalyst	ORR activity at 0.9V		ORR activity at $E_{1/2}$		E_{onset}	Number of electrons	Tafel Slope (mV/dec)
	Mass Activity (mA/mg_{PGM})	Specific Activity (mA/cm^2)	Mass Activity (mA/mg_{PGM})	Specific Activity (mA/cm^2)			
Pt	79	0.52	16 (0.90 V)	0.12	1.02	3.6	76
Pd	11.3	0.05	11.3 (0.84 V)	0.05	0.92	2.5	87
PtPd 3:1	253	0.44	29 (0.93V)	0.05	1.11	3.7	70
PtPd 1:3	84	0.22	26 (0.89V)	0.051	0.99	3.8	68
PtPd 1:1	203	0.39	39 (0.91V)	0.076	0.99	3.5	65

Table 7.4 Electrochemical Kinetic properties of other papers considering pure Pt, pure Pd and their bimetallic alloys on different analogies.

Catalyst	**Potential activities acquired**	**Mass Activity (mA/mg_{PGM})**	**Specific Activity (mA/cm^2)**	**Slope**	**Source**
Pt	0.88V	138.4	0.155	-	[71]
$Pt_{40}Pd_{60}$		107.2	0.448	-	
Pt_1Pd_2/C	0.90V	367	0.046	88.6	[72]
Pt_1Pd_3/C		197	0.124	82.6	
Pt/XC-72R	0.85V	-	0.0246	-	[73]
Pt_2Pd_1/C		-	0.0397	-	
Pt_1Pd_1/C		-	0.0295	-	
Pt_1Pd_3/C		-	0.0175	-	
Pt nanocubes	0.90V	-	0.113	58	[74]
Pd nanocubes		-	0.078	64	
$Pt_{64}Pd_{36}$		-	0.089	62	
$Pt_{46}Pd_{54}$		-	0.072	62	
$Pt_{28}Pd_{72}$		-	0.070	66	
Pt	0.80V	14.6	-	-	[75]
Pd		29.8	-	-	
$Pt_{25}Pd_{75}$		41.7	-	-	
$Pt_{47}Pd_{53}$		12.5	-	-	
$Pt_{77}Pd_{23}$		10.7	-	-	

Also results from other papers, on the same topic of ORR, are included, so they can be discussed and compared with our own experimental values. This comparison

can provide us an assessment on the efficiency and performance of our electrocatalysts.

7.2.1 Conditioning procedure

Cyclic voltammetry, for the Pt_xPd_y bimetallic catalysts, was conducted under N_2-saturated 0.1 M $HClO_4$ aqueous solution for 30 min (75 cycles) at 100 mV s^{-1}. In the following diagrams we can distinguish the procedure of 'conditioning' and what changes inflicted on the ECSA of our catalysts.

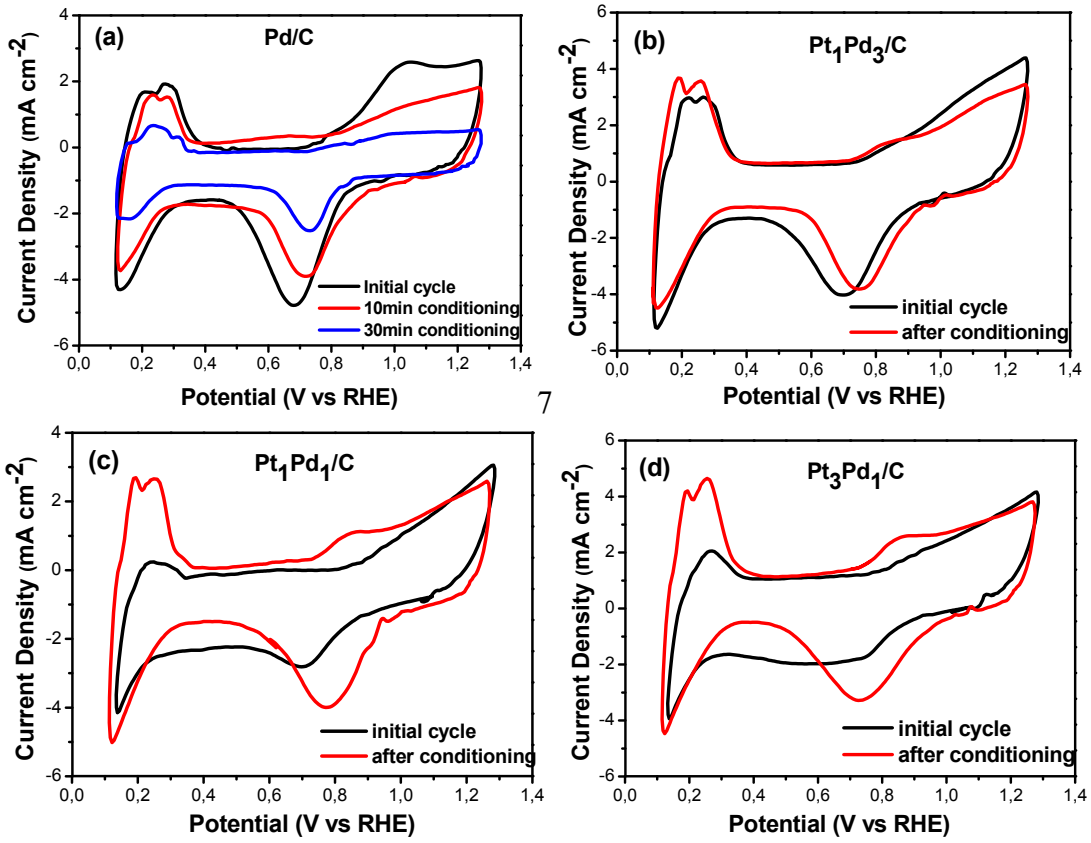

Figure 7.8 CV curves before and after conditioning in N2-saturated 0.1 M HClO4 aqueous solution, at a scan rate of 50 mV s-1 for (a) Pd/C, (b) Pt_1Pd_3/C, (c) Pt_1Pd_1/C and (d) Pt_3Ir_1/C (20 wt%).

Starting from pure Pd (Fig. 7.8 a.), we can see that in the potential range of 0.1 to 0.4 V vs. RHE, large peaks are formed, which normally correspond to the hydrogen adsorption/desorption phenomena. From the average surface of these 2 peaks (upper and bottom), ECSA is calculated (228 cm^2/mg_{Pd}). Also, the oxide formation/reduction regions are distinguished, onset potential of the oxide reduction is estimated at 0.90V (negative scanning) and onset of surface oxidation at 0.7V (positively scanning). Although we would normally expect the catalyst, Pd, to increase its ECSA, during conditioning under N_2, that is not happening. In the CV, as the conditioning

progresses, we can clearly see ECSA decreasing. Literature states that the hydrogen desorption and oxide reduction regions should be increasing, during cycling, while hydrogen adsorption region decreases until stabilization [76]. So, our results state that our 20wt% Pd catalyst is unstable and deteriorates very fast without any significant constrain.

Pt_1Pd_3, on the other hand, follows a standard CV path, Fig 7.8b, stabilizing almost on its initial state. As a result of the chloride contained in the electrolyte, oxidizing regions appear, following both Pt's and Pd's tendency to form the so called surface 'oxide', [77, 78]. Specifically, hydrogen adsorption (H_{ad}) and hydrogen desorption (H_{des}) areas appear between 0.1 and 0.38 V, oxide formation starts at 0.7 V and oxide reduction begins at 1.0 V. The ECSA (503 cm^2/mg_{PGM}) is significantly larger than pure Pd, indicating more active sites on this catalyst, coincident with the Pt binding theory. Like pure Pd, Pt_1Pd_3's electrochemical active surface could have been extracted without CV conditioning, which is a result of the Pd being the prevailing term (75% of this catalyst).

On Pt-Pd (1:1) (Fig. 7.8c.), we observe that the shape of CV, after conditioning, remains almost identical with the Pt_1Pd_3 one, as a result their H_{ad} and H_{des} areas, oxide formation area's and oxide reduction area's limits are close. Pt_1Pd_1, above mentioned areas, appear from 0.12 to 0.40 V, 0.75V and 0.95V (vs RHE) respectively. Unlike Pt_1Pd_3, Pt_1Pd_1 acquired its final ESCA after conditioning, because of Pd not being any more the prevailing electrocatalyst. Pt_1Pd_1 ECSA is slightly increased (516 cm^2/mg_{PGM}), compared to Pt_1Pd_3. This indicates that with less Pt and more Pd we can achieve the same active sites.

Finally, in the Pt-Pd (3:1) (Fig. 7.8d.), the H_{ad} and H_{des} areas appear between 0.12 to 0.40 V, oxide formation starting at 0.75V and oxide reduction beginning at 1.05V (vs RHE), which are also well matching with Pt_1Pd_1 and Pt_1Pd_3 areas. The ECSA of Pt_3Pd_1, 583 cm^2/mg_{PGM} of catalyst, it's the biggest among the Pt_xPd_y bimetallic catalysts and their pure forms (Pt and Pd), meaning that Pt needs only a little quantity of Pd catalyst, alloyed with it, in order to promote its active sites.

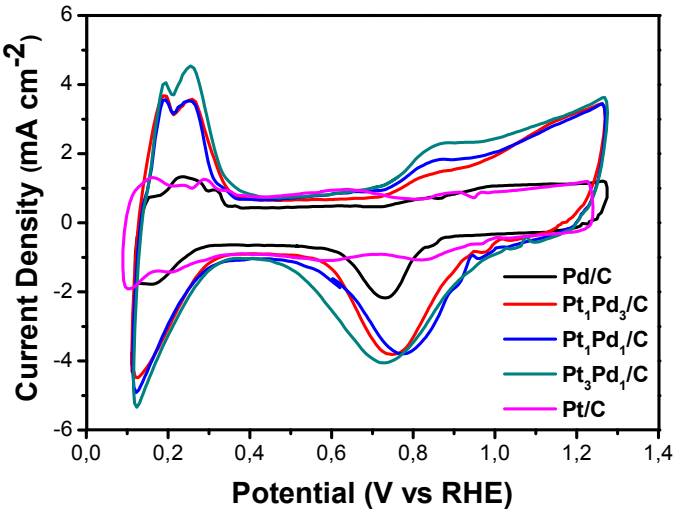

Figure 7.9 CV curves in N2-saturated 0.1 M HClO4 aqueous solution, at 50 mV s^{-1}.

Concluding about ECSA, from Fig. 7.9, we can deduce that the pure Pd and Pt have much smaller ECSA than their bimetallic compounds, which is confirmed by the Pt binding theory on how pure metals, like Pt and Pd, bind oxygen too strong, thus decreasing their electrochemical active surface (which is covered by oxygen intermediate species).

7.2.2 Oxygen Reduction Reaction (ORR) Kinetics

The ORR activity of the tested electrocatalysts was examined by rotating disk electrode (RDE) experiments, from which the corresponding linear sweep voltammetry (LSV) curves were taken. All RDE experiments were conducted under O_2-saturated 0.1 M $HClO_4$ aqueous solution, at a scan rate of 20 mV s^{-1}, at rotation rates from 400 rpm to 2000 rpm. In Fig. 7.10, the LSV curves and the Koutecky-Levich (K-L) plots for Pd and Pt_xPd_y are presented. K-L plots are derived from the Koutecky-Levich equation (7.2) in the range of potentials from 0.6 to 1.0 V vs RHE. The slope of K-L diagrams is further used to determine the number of electrons transferred per oxygen molecule for the ORR, through equation (7.3).

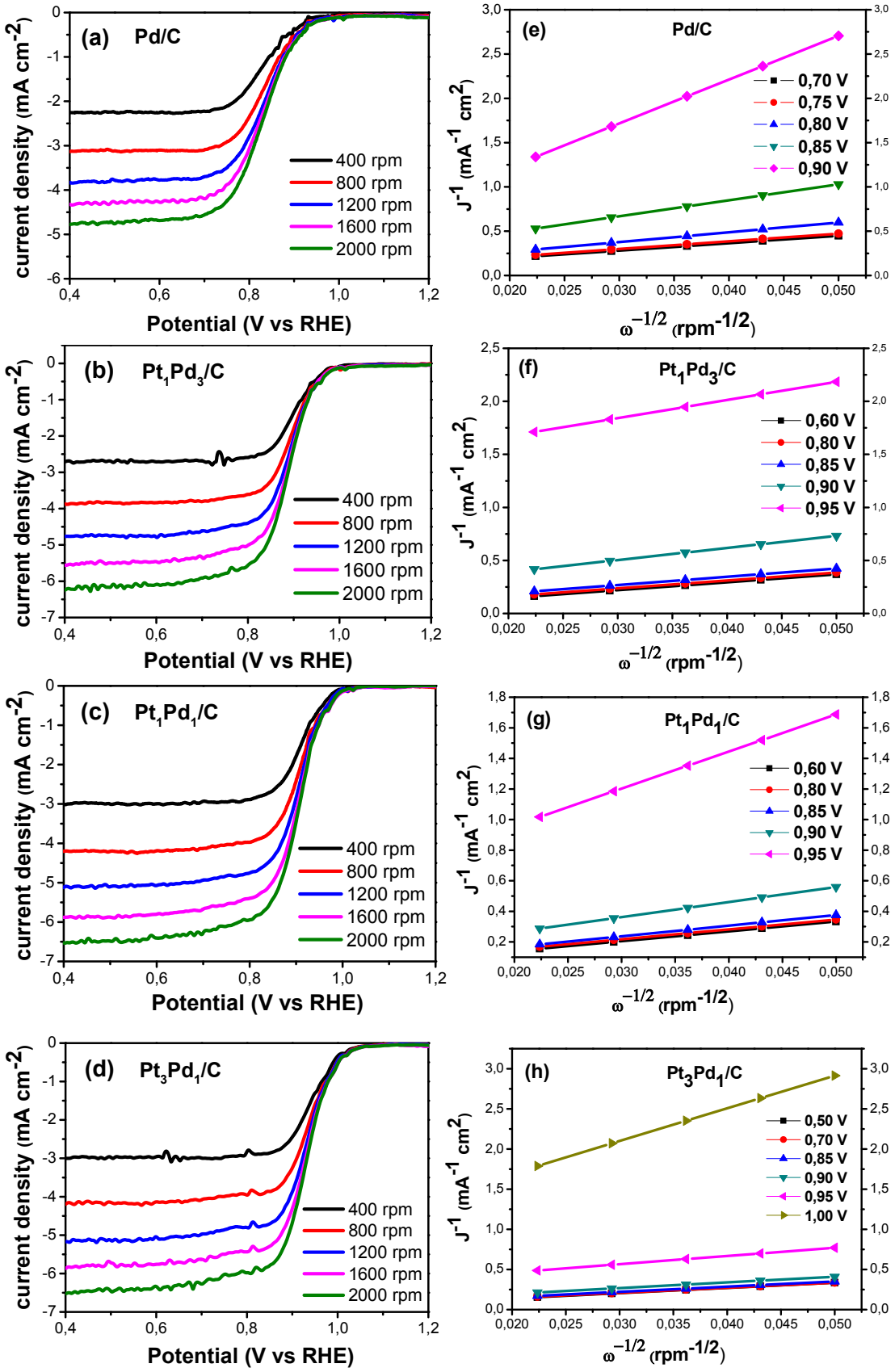

Figure 7.10 LSV curves in O_2-saturated 0.1 M $HClO_4$ aqueous solution, at rotation rates from 400 to 2000 rpm, at a scan rate of 20 mV s^{-1} for (a) Pd/C, (b) Pt_1Pd_3/C, (c) Pt_1Pd_1/C and (d) Pt_3Pd_1/C. Koutecky-Levich plots for (e) Pd/C, (f) Pt_1Pd_3/C, (g) Pt_1Pd_1/C and (h) Pt_3Pd_1/C.

As pointed in the conditioning procedure results, pure Pd is unstable and that can be understood also by comparing LSV plots before and after condition. In Fig.7.11 we observe deterioration in both kinetic and mass transfer region of the reaction, with a loss of 1.23 mA/cm^2 at the half wave potential of 0.9V vs RHE. LSV experiments on ascending rpm (Fig. 7.10a.), were conducted after the catalyst was undergone conditioning, as an outcome final results are not optimal. Furthermore, according to Koutecky-Levich results, the ORR for the Pd proceeds via 2-electron pathway, indicating sluggish reaction kinetics.

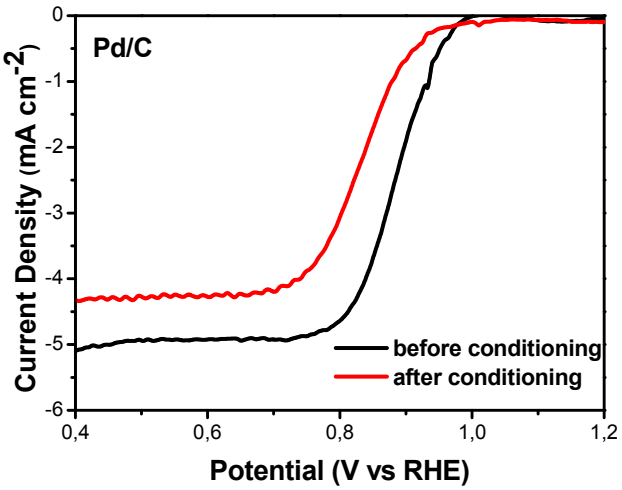

Figure 7.11 LSV curves in O_2-saturated 0.1 M $HClO_4$ aqueous solution, at rotation rate of 1600 rpm, at a scan rate of 20 mV s^{-1}, before and after condition of pure Pd 20 wt% on Vulcan XC-72.

LSV plots for Pt_1Pd_3 (Fig. 7.10b.), exhibit an onset potential of 0.99V and a current density at mass control region of 5.46 mA/cm^2 (1600rmp). Comparing to pure Pd, just by the addition of small portion of Pt, this catalyst (Pt_1Pd_3) exhibits better kinetic parameters. As we can notice from table 7.3, Pt_1Pd_3 has 7 times higher mass activity and 5 times higher specific activity than pure Pd at 0.9V. The reaction, as extracted from the Koutecky-Levich plots, proceeds in 4 electron path which is desired, unlike Pd 2-electron path.

Pt_1Pd_1 LSV plots display an onset potential of 0.99V and 5.9mA/cm^2 limiting diffusion current at 1600rpm. Pt_1Pd_1 has superior kinetics compared to Pt_1Pd_3, it has in fact at least two times higher mass (203 mA/mg$_{PGM}$) and specific (0.39 mA/cm^2) activity than Pt_1Pd_3, shown on table 7.3. Resulting from the Koutecky-Levich plots and equations, the mechanism here also proceeds with 4 electrons, indicating fast kinetics and water as a product.

Pt_3Pd_1 LSV obtained at different rpm, exhibit a plateau of 5.83 mA/cm^2 on 1600rpm.Except from a good limiting diffusion current also Pt_3Pd_1 has the fastest onset potential (1.1 V vs RHE), meaning current can be achieved with just a minimum overpotential. Its kinetic parameters, (table 7.3) resemble those of Pt_1Pd_1, 253 mA/mg$_{PGM}$ mass activity and 0.44 mA/cm^2 specific activity, in fact they are slightly higher but that comes with the cost of adding more Pt. As expected, this catalyst also proceeds on a 4-electron path.

7.2.3 Pt_xPd_y summary

According to the Tafel plots presented in Fig. 7.12a., for pure Pt, Pd and bimetallic Pt_xPd_y, Pt_1Pd_1 presents the lowest Tafel slope (65 mV/dec). Since the smaller the slope, the less the overpotential increases with the current density, it is concluded that Pt_1Pd_1 exhibits the highest ORR electrocatalytic activity among the tested catalysts, , followed in sequence by Pt_1Pd_3, Pt_3Pd_1, Pt, Pd.

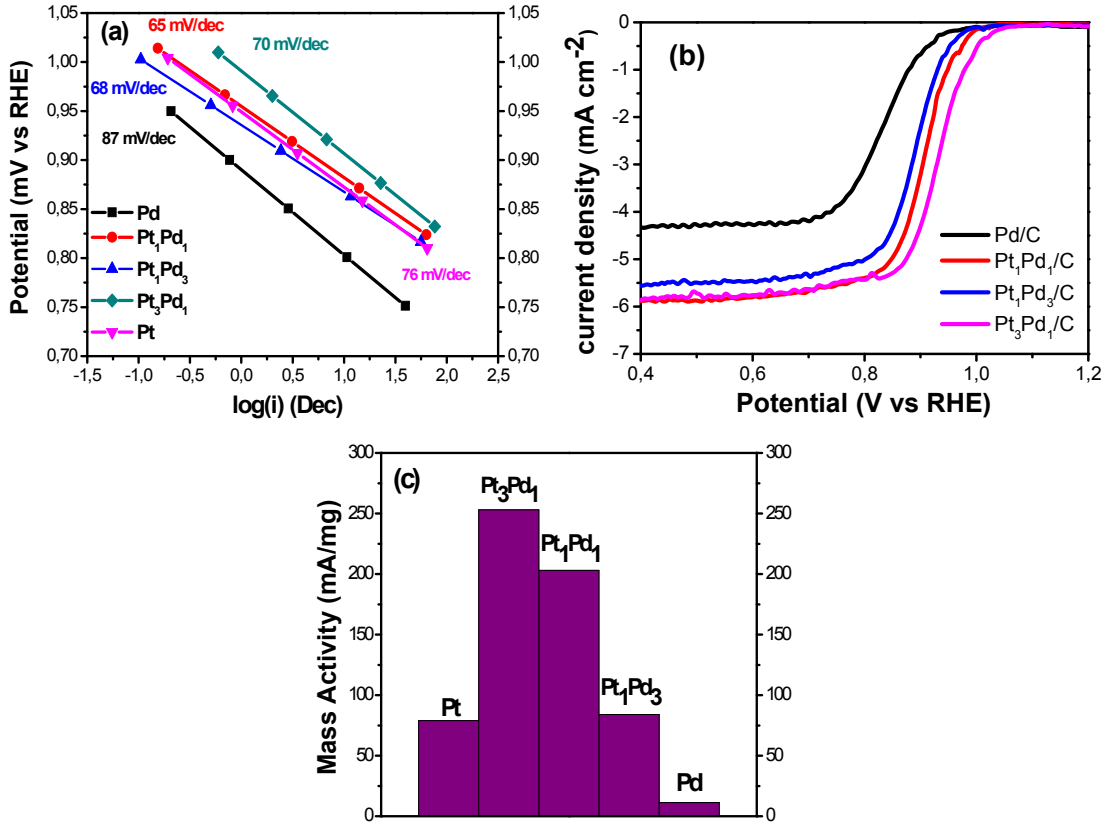

Figure 7.12 (a) Tafel plots at low overpotentials, (b) LSV curves in O_2-saturated 0.1 M $HClO_4$ aqueous solution, at rotation rate of 1600 rpm, at a scan rate of 20 mV s^{-1}, (c) Mass Activities at 0.9V vs RHE for 20 wt% Pt, Pt_3Pd_1, Pt_1Pd_1, Pt_3/Pd_1 and Pd on Vulcan XC-72.

LSV plots (Fig. 7.12 b.), give us an initiatory view about current density, on 0.9V (kinetic controlled region) it follows a descending path of Pt_3Pd_1 (4mA/cm^2) > Pt_1Pd_1

(3.2 mA/cm^2) > Pt (2.6 mA/cm^2) > Pt_1Pd_3 (2.2 mA/cm^2) > Pd (1.9 mA/cm^2). These results though are not fully representative, so we also need to compare their mass and specific activities, as well as their Tafel slopes mentioned before.

Their mass activity (mA/mg_{PGM}) goes like Pt_3Pd_1 (253mA/mg_{PGM}) > Pt_1Pd_1 (203mA/mg_{PGM}) > Pt_1Pd_3 (84 mA/mg_{PGM}) > Pt (79 mA/mg_{PGM}) > Pd (11.3 mA/mg_{PGM}). Their specific activity is as follows: Pt (0.52mA/cm^2) > Pt_3Pd_1 (0.44 mA/cm^2) > Pt_1Pd_1 (0.39 mA/cm^2) > Pt_1Pd_3 (0.22 mA/cm^2) > Pd (0.05 mA/cm^2). The only strange thing we can observe is that Pt has actually the best specific activity which is owed to its small ECSA calculated from the CV at the beginning.

According to the extracted results presented above, it is concluded that pure Pd is not favorable for the ORR, due to its low mass and specific activities. Compared to Pd, Pt and Pt_1Pd_3 catalysts exhibit higher electrocatalytic activity for the ORR. More precisely, Pt exhibits the highest specific activity, while Pt_1Pd_3 presents the lowest Tafel slope and the highest mass activity, as it shown on table 7.3. Finally, Pt_1Pd_1 and Pt_3Pd_1 are the most sufficient for the ORR, among the tested catalysts, according to their activities; their mass activities are at least 2 times higher compared to Pd, Pt and Pt_1Pd_3 catalysts (Fig. 7.12 c.). Furthermore, their exhibited low Tafel slopes imply superior kinetics; Pt_1Pd_1 slope is close to 60mV/dec (Fig. 7.12 a.), indicating 4-electron pathway for the ORR.

CHAPTER VIII

COMPARISON OF THE ELECTROCATALYSTS TESTED

8.1 Comparison of ORR electrocatalytic activities

In this chapter a comparison between the tested catalysts is made, based on the loading percentage of platinum on the bimetallic electrocatalysts. Initially, pure Pt, Pd and Ir catalysts were compared, as it can be seen from the LSV curves of Fig. 8.1a., Ir exhibits the lowest ORR activity as it presents the less positive onset potential. Furthermore, it is unstable as it does not acquire a flat plateau at the mass transport control region. Pt, as it was expected from the literature, presents the highest ORR activity among the three electrocatalysts, with the highest onset and half wave potentials as well as the highest limiting current. Its mass activity was found to be 79.4 mA mg_{PGM}^{-1}.

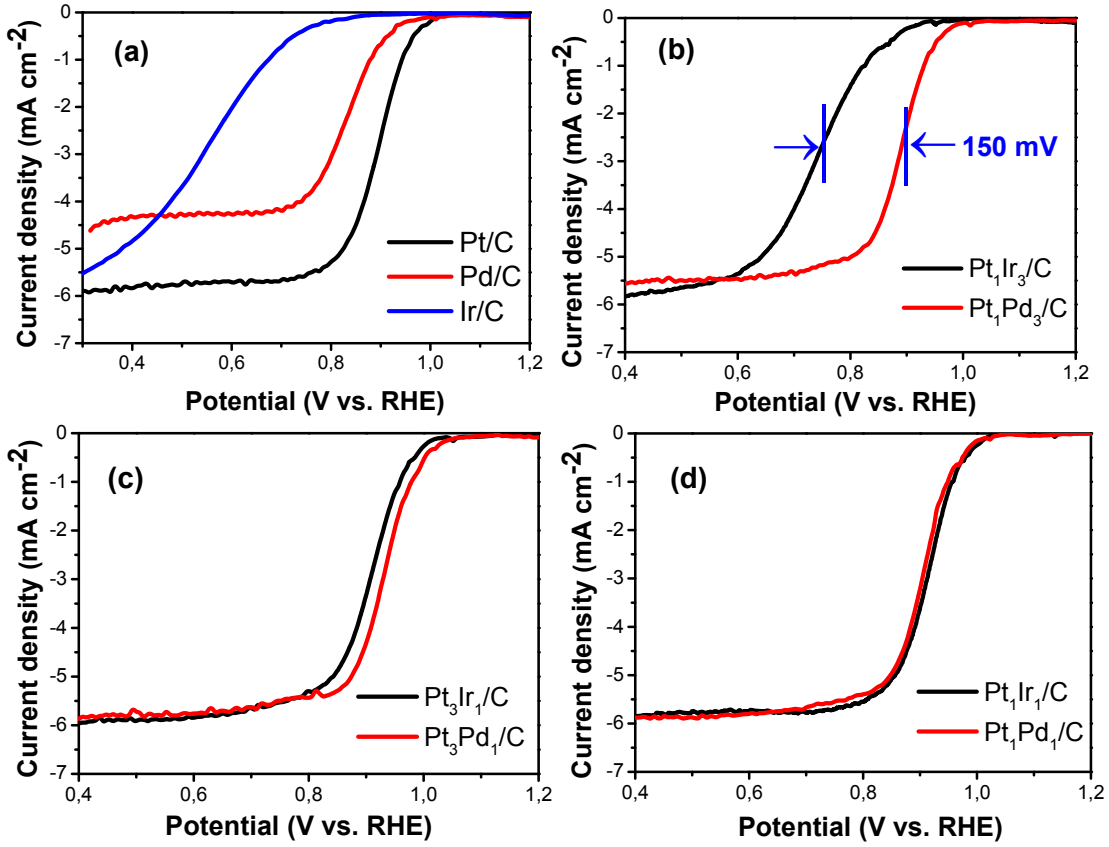

Figure 8.1 LSV curves in O_2-saturated 0.1 M $HClO_4$ aqueous solution, at rotation rate of 1600 rpm, at a scan rate of 20 mV s^{-1} for (a) pure Pt, Pd and Ir, (b) Pt_1Ir_3 and Pt_1Pd_3, (c) Pt_3Ir_1 and Pt_3Pd_1, (d) Pt_1Ir_1 and Pt_1Pd_1.

Also, from Fig. 8.1a., it is shown clearly that Pd catalyst presents higher ORR activity than Ir, with a much more positive onset potential and a steady plateau at the mass transport control region. However, as it is shown on Fig.8.2a., compared to Pt its mass activity is 7 times lower (11.3 mA mg_{PGM}^{-1}).

In the case of bimetallic catalysts with a loading percentage of Ir and Pd equal to 75%, the electrocatalytic activity, towards ORR, of Pt_1Pd_3 was higher than Pt_1Ir_3. Still Pt_1Ir_3 was stable compared with pure Ir, reaching a plateau at the mass transport control region. The difference of their ORR activity it can be clearly seen from Fig. 8.1b., observing the earlier onset potential of Pt_1Pd_3 and their difference of their half wave potentials (150 mV vs RHE).

When Pt is the dominant part in the bimetallic catalysts, with an atomic ratio 3:1, we can observe from Fig. 8.1c. that Pt_3Pd_1 exhibits more positive onset potential than Pt_3Ir_1, predicting that its mass activity is going to be higher. This prediction comes up from the fact that their mixed control regions have almost the same inclination, and their limiting currents are about equal (~6 mA cm^{-2}). The above assumption was confirmed by the electrochemical characterizations made to the previous chapter, where it was resulted almost a doubly mass activity of Pt_3Pd_1 compared with Pt_3Ir_1 (253 and 123 mA mg_{PGM}^{-1} respectively, Fig. 8.2a.). Regarding their specific activities, Pt_3Pd_1 has a slightly higher value than Pt_3Ir_1 (0.44 and 0.41 mA cm^{-2} respectively), fact that has been attributed to the smaller ECSA of Pt_3Ir_1. Finally, comparing their Tafel slopes, Pt_3Ir_1 showed slightly better ORR activity at the kinetic region as its Tafel slope is about 4 mV/dec smaller than Pt_3Pd_1 (Fig. 8.2b.).

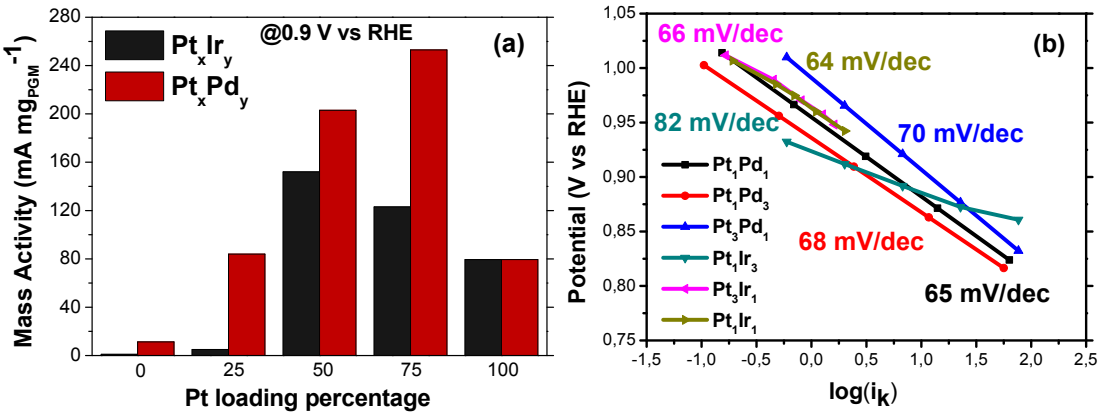

Figure 8.2 a) Mass activities at 0.9 V vs RHE and b) Tafel plots at low overpotentials for Pt_xIr_y and Pt_xPd_y.

8.2 Durability results

Pt_1Ir_1 and Pt_1Pd_1 were selected among the tested electrocatalysts as the best ones considering their mass and specific activities as well as their Tafel slopes (Fig. 8.2). These two bimetallic electrocatalysts, and Pt as a standard of comparison, underwent durability tests in order to determine their long-term stability for fuel cell applications. The durability of Pt_1Ir_1 and Pt_1Pd_1, compared with Pt, was evaluated by accelerated durability test (ADT), by cycling the catalysts between 0.6 and 1.0 V vs RHE, in O_2-saturated 0.1 M $HClO_4$ aqueous solution, at a scan rate of 100 mV s^{-1}, at 1600 rpm for 5000 cycles. Afterwards, catalysts were refreshed by undergoing CV from 0.15 to 1.25 V vs RHE, in O_2-saturated solution, and subsequently their LSV curves were obtained (Fig. 8.3).

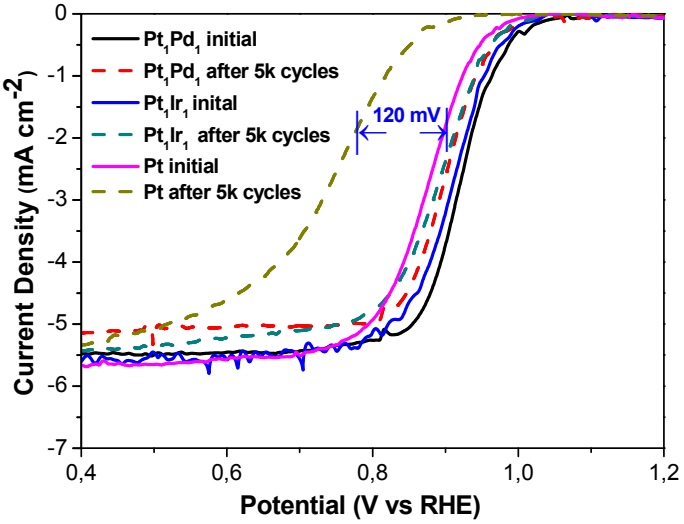

Figure 8.3 LSV curves before and after 5k potential cycles in O_2-saturated 0.1 M $HClO_4$ aqueous solution, with a scan rate of 100 mV s^{-1}, at rotation rate of 1600 rpm for Pt, Pt_1Ir_1 and Pt_1Pd_1

At first glance, from Fig. 8.3, it can be clearly stated that Pt was deteriorated radically in its kinetic region. More precisely, after the durability test a negative shift of 120 mV vs RHE was revealed, to reach the current that obtained before the ADT at 0.9 V vs RHE. Pt_1Pd_1 and Pt_1Ir_1 exhibited similar behavior after the durability tests as both shifted negatively approximately 23 mV vs RHE. In terms of mass activities, Pt, Pt_1Pd_1 and Pt_1Ir_1 displayed a loss percentage of 99%, 52% and 44% respectively.

According to the literature the enhanced stability of the bimetallic catalysts, compared to Pt, can be explained by the fact that Pt associates oxygen species too strongly, leading to fatigue, and as an outcome it is incapable of refreshing back near to its initial state. Bimetallic catalysts avoid this phenomenon by the dissolution of the alloyed metal on Pt. Therefore, we can determine that Pt_1Ir_1 and Pt_1Pd_1 are capable of performing in fuel cell conditions without showing any serious case of diminishing in their ORR performance.

CHAPTER IX

CONCLUNDING REMARKS

In this work, the ORR electrocatalytic activity over Pt, Ir, Pd, Pt_xIr_y and Pt_xPd_y supported on Vulcan XC-72 (20 wt%, with x:y atomic ratios 3:1, 1:1, 1:3) electrocatalysts was examined for the purpose of enhancing the oxygen reduction reaction on fuel cell applications. Pt, the most commonly used electrocatalyst for the ORR, was used as a standard of comparison for the rest of the tested catalysts. From the electrochemical characterizations, Pt was found to exhibit decent electrochemical performance, with mass activity 79.4 mA mg_{PGM}^{-1} and specific activity 0.52 mA cm^{-2} at 0.9 V vs RHE. Its Tafel slope was estimated at 71.8 mV/dec, confirming the results from the Koutecky-Levich analysis that ORR with pure Pt proceeds via 4-electron pathway.

The results showed that pure Ir exhibited deficient electrocatalytic performance, considering its low onset potential and its instability, as it did not reach a flat plateau at the mass transport control region. However, from the electrochemical characterizations it was concluded that Ir in a metal loading percentage equal to or less than 50% at bimetallic Pt_xIr_y catalysts, contributes to the enhancement of the ORR electrocatalytic activity, compared with Pt. More precisely, Pt_1Ir_1 was found to be the most favorable for the oxygen reduction reaction, according to its mass (152 mA mg_{PGM}^{-1}) and specific activity (0.55 mA cm^{-2}), as well as its Tafel slope (64.3 mV/dec). Pure Pd catalyst was evaluated as unstable because of its fast deterioration during conditioning in N2-saturated 0.1 M HClO4 aqueous solution, at a scan rate of 50 mV s^{-1}. This behavior corresponds with the low exhibited values of mass and specific activities, as well as its Tafel slope (87 mV/dec), which indicates that the ORR tends to proceed via 2-electron pathway. On the other hand, all the bimetallic Pt_xPd_y catalysts displayed larger mass activities than Pt. Specifically, Pt_3Ir_1 mass activity (253 mA mg_{PGM}^{-1}) was found to be three times and twenty times larger than Pt and Pd mass activities respectively. Furthermore, their Tafel slopes were close to 70 mV/dec, indicating superior kinetics, and a 4-electron pathway for the ORR, with Pt_1Pd_1 exhibiting the lowest (65 mV/dec).

Among the tested electrocatalysts, Pt_1Ir_1 and Pt_1Pd_1 were distinguished as the most favorable for the ORR, considering concurrently their electrocatalytic activities and their behavior under accelerated durability test (ADT). Both of them exhibited superior mass (152 and 203 mA mg_{PGM}^{-1} respectively) and specific (0.55 and 0.39 mA cm^{-2}) activities, and also their deterioration after the ADT for 5000 potential scanning cycles were at low levels (52% and 44% loss percentage of mass activities).

By those electrochemical characterizations can be determined the suitability of the catalysts for real time operation on fuel cells but this study it is not yet fully integrated. Further experiments must be conducted inside a working fuel cell in order to obtain a complete view of the catalysts. Parameters like temperature, hydrogen deprivation and water flooding must be considered before reaching a verdict. Physicochemical characterizations, such as X-ray diffraction (XRD), scanning electron microscopy (SEM) and transmission electron microscopy (TEM) should also be conducted to determine the morphology of the surfaces of the catalysts. An extra factor that effects the selection of the electrocatalyst for the ORR is the cost of the noble metals. Commonly, Platinum was the most expensive metal among those who presented high ORR activity, nowadays though Palladium and Iridium prices have skyrocketed, making them less favorable for materials such as electrocatalysts.

REFERENCES

[1] B. Long, H. Yang, M. Li, M.-S. Balogun, W. Mai, G. Ouyang, Y. Tong, P. Tsiakaras and S. Song, Applied Catalysis B: Environmental, 243 (2019) 365.
[2] IEA, Electricity Statistics, 2019.
[3] IEA, Energy Snapshot, 2019.
[4] T.U. Daim, J. Kim, I. Iskin, R.A. Taha and K.C. van Blommestein, Policies and programs for sustainable energy innovations, 2015.
[5] R. Prakash and I.K. Bhat, Renewable and sustainable energy reviews, 13 (2009) 2716.
[6] J. Lu, Z. Tang, L. Luo, S. Yin, P.K. Shen and P. Tsiakaras, Applied Catalysis B: Environmental, 255 (2019) 117737.
[7] A. Albarbar, Proton Exchange Membrane Fuel Cells, Springer, 2017.
[8] A.J. Bard, L.R. Faulkner, J. Leddy and C.G. Zoski, Electrochemical methods: fundamentals and applications, wiley New York, 1980.
[9] D.D. Ebbing and S.D. Gammon, General chemistry, 2017.
[10] J.R. Miller and P. Simon, Science, 321 (2008) 651.
[11] T. Christen and M.W. Carlen, Journal of power sources, 91 (2000) 210.
[12] M. Choun, Investigation on formate oxidation on palladium and strategies for improving performance in alkaline direct formate fuel cells, 2017.
[13] A. González, E. Goikolea, J.A. Barrena and R. Mysyk, Renewable and sustainable energy reviews, 58 (2016) 1189.
[14] R. Kötz and M. Carlen, Electrochimica acta, 45 (2000) 2483.
[15] R.N.A.R. Seman, M.A. Azam and M.H. Ani, Nanotechnology, 29 (2018) 502001.
[16] M. Zhi, C. Xiang, J. Li, M. Li and N. Wu, Nanoscale, 5 (2013) 72.
[17] U. Guth, W. Vonau and J. Zosel, Measurement Science and Technology, 20 (2009) 042002.
[18] M. Dong, C. Zhang, M. Ren, R. Albarracín and R. Ye, Sensors, 17 (2017) 2627.
[19] D. Grieshaber, R. MacKenzie, J. Vörös and E. Reimhult, Sensors, 8 (2008) 1400.
[20] N.R. Stradiotto, H. Yamanaka and M.V.B. Zanoni, Journal of the Brazilian Chemical Society, 14 (2003) 159.
[21] B. Pejcic and R. De Marco, Electrochimica acta, 51 (2006) 6217.
[22] J.-M. Tarascon and M. Armand, Materials for Sustainable Energy: A Collection of Peer-Reviewed Research and Review Articles from Nature Publishing Group, World Scientific, 2011, p. 171.
[23] M. Winter and R.J. Brodd, Chemical reviews, 105 (2005) 1021.
[24] D.L. Anderson and D. Patiño-Echeverri, Duke University, (2009).
[25] B. Scrosati and J. Garche, Journal of power sources, 195 (2010) 2419.
[26] G.E. Blomgren, Journal of The Electrochemical Society, 164 (2017) A5019.
[27] E.I. Ortiz-Rivera, A.L. Reyes-Hernandez and R.A. Febo, 2007 IEEE Conference on the History of Electric Power 2007.
[28] J.M. Andújar and F. Segura, Renewable and sustainable energy reviews, 13 (2009) 2309.
[29] J. Zhang, PEM fuel cell electrocatalysts and catalyst layers: fundamentals and applications, Springer Science & Business Media, 2008.
[30] L. Putilov, A. Demin, V. Tsidilkovski and P. Tsiakaras, Applied energy, 242 (2019) 1448.

[31] Z. Qi, Proton exchange membrane fuel cells, CRC Press, 2013.
[32] A. Kirubakaran, S. Jain and R. Nema, Renewable and sustainable energy reviews, 13 (2009) 2430.
[33] V. Mehta and J.S. Cooper, Journal of power sources, 114 (2003) 32.
[34] A. El-Kharouf, A. Chandan, M. Hattenberger and B. Pollet, Journal of the Energy Institute, 85 (2012) 188.
[35] S. Zhang, X.-Z. Yuan, J.N.C. Hin, H. Wang, K.A. Friedrich and M. Schulze, Journal of power sources, 194 (2009) 588.
[36] R. Vadivelan and S. Kumar, IOSR Journal of Mathematics 2015.
[37] L. Cindrella, A.M. Kannan, J. Lin, K. Saminathan, Y. Ho, C. Lin and J. Wertz, Journal of power sources, 194 (2009) 146.
[38] D. Fadzillah, M.I. Rosli, M.Z.M. Talib, S.K. Kamarudin and W.R.W. Daud, Renewable and sustainable energy reviews, 77 (2017) 1001.
[39] A. Hermann, T. Chaudhuri and P. Spagnol, International journal of hydrogen Energy, 30 (2005) 1297.
[40] Y. Wang, K.S. Chen, J. Mishler, S.C. Cho and X.C. Adroher, Applied energy, 88 (2011) 981.
[41] F. Barbir, PEM fuel cells: theory and practice, Academic Press, 2012.
[42] F. Si, Y. Zhang, L. Yan, J. Zhu, M. Xiao, C. Liu, W. Xing and J. Zhang, Rotating Electrode Methods and Oxygen Reduction Electrocatalysts, Elsevier, 2014, p. 133.
[43] M. Shao, Q. Chang, J.-P. Dodelet and R. Chenitz, Chemical reviews, 116 (2016) 3594.
[44] J.O.M. Bockris, Comprehensive treatise of electrochemistry, Plenum Press, New York, 1980.
[45] A.M. Gómez-Marín, R. Rizo and J.M. Feliu, Beilstein journal of nanotechnology, 4 (2013) 956.
[46] A.M. Gómez-Marín, R. Rizo and J.M. Feliu, Catalysis Science & Technology, 4 (2014) 1685.
[47] F.C. Store, Considerations for Fuel Cell Design, 2017.
[48] Y. Nie, L. Li and Z. Wei, Chemical Society Reviews, 44 (2015) 2168.
[49] H.S. Wroblowa and G. Razumney, Journal of Electroanalytical Chemistry and Interfacial Electrochemistry, 69 (1976) 195.
[50] D. Thompsett, Handbook of Fuel Cells, (2010).
[51] Z. Meng, S. Cai, R. Wang, H. Tang, S. Song and P. Tsiakaras, Applied Catalysis B: Environmental, 244 (2019) 120.
[52] H. Du, K. Wang, P. Tsiakaras and P.K. Shen, Applied Catalysis B: Environmental, 258 (2019) 117951.
[53] A. Morozan, B. Jousselme and S. Palacin, Energy & Environmental Science, 4 (2011) 1238.
[54] S. Jing, D. Wang, S. Yin, J. Lu, P.K. Shen and P. Tsiakaras, Electrochimica acta, 298 (2019) 142.
[55] H.-y. Lei, J.-h. Piao, A. Brouzgou, E. Gorbova, P. Tsiakaras and Z.-x. Liang, International journal of hydrogen Energy, 44 (2019) 4423.
[56] D. Wei, Y. Liu, Y. Wang, H. Zhang, L. Huang and G. Yu, Nano letters, 9 (2009) 1752.
[57] Y. Li, W. Zhou, H. Wang, L. Xie, Y. Liang, F. Wei, J.-C. Idrobo, S.J. Pennycook and H. Dai, Nature nanotechnology, 7 (2012) 394.
[58] A. Brouzgou, E. Gorbova, Y. Wang, S. Jing, A. Seretis, Z. Liang and P. Tsiakaras, Ionics, (2019) 1.

[59] X. Zhou, J. Qiao, L. Yang and J. Zhang, Advanced Energy Materials, 4 (2014) 1301523.
[60] F. Scholz, Electroanalytical Methods Guide to Experiments and Applications, Springer Berlin, Berlin, 2014.
[61] G. Denuault, M. Sosna and K.-J. Williams, Handbook of Electrochemistry, Elsevier, 2007, p. 431.
[62] Urrjaa, Cyclic Voltammetry, 2013.
[63] A. Brajter-Toth, Electroanalytical Methods: Guide to Experiments and Applications Edited by Fritz Scholz (E.-M.-Arndt-Universität Greifswald). Springer-Verlag: Berlin, Heidelberg, New York. 2002. xxii+ 332 pp. $69.95. ISBN 3-540-42229-3, ACS Publications, 2003.
[64] W. Wang, X. Wei, D. Choi, X. Lu, G. Yang and C. Sun, Advances in Batteries for Medium and Large-Scale Energy Storage, Elsevier, 2015, p. 3.
[65] K. Scott and E.H. Yu, Microbial electrochemical and fuel cells: fundamentals and applications, Woodhead Publishing, 2015.
[66] K. Shinozaki, J.W. Zack, R.M. Richards, B.S. Pivovar and S.S. Kocha, Journal of The Electrochemical Society, 162 (2015) F1144.
[67] M. Łukaszewski, M. Soszko and A. Czerwiński, Int. J. Electrochem. Sci, 11 (2016) 4442.
[68] F. Tzorbatzoglou, A. Brouzgou and P. Tsiakaras, Applied Catalysis B: Environmental, 174 (2015) 203.
[69] T. Ioroi and K. Yasuda, Journal of The Electrochemical Society, 152 (2005) A1917.
[70] S.J. Hwang, S.J. Yoo, T.-Y. Jeon, K.-S. Lee, T.-H. Lim, Y.-E. Sung and S.-K. Kim, Chemical Communications, 46 (2010) 8401.
[71] J. Zhao and A. Manthiram, Applied Catalysis B: Environmental, 101 (2011) 660.
[72] S. Thanasilp and M. Hunsom, Renewable Energy, 36 (2011) 1795.
[73] W. He, J. Liu, Y. Qiao, Z. Zou, X. Zhang, D.L. Akins and H. Yang, Journal of power sources, 195 (2010) 1046.
[74] K. Jukk, N. Kongi, K. Tammeveski, J. Solla-Gullón and J.M. Feliu, Electrochemistry Communications, 56 (2015) 11.
[75] A.B. Papandrew, C.R. Chisholm, S.K. Zecevic, G.M. Veith and T.A. Zawodzinski, Journal of The Electrochemical Society, 160 (2013) F175.
[76] R. Rahul, R. Singh, B. Bera, R. Devivaraprasad and M. Neergat, Physical Chemistry Chemical Physics, 17 (2015) 15146.
[77] A. Berná, V. Climent and J.M. Feliu, Electrochemistry Communications, 9 (2007) 2789.
[78] R. Wu, P. Tsiakaras and P.K. Shen, Applied Catalysis B: Environmental, 251 (2019) 49.